2. Experimental

2.1 X-Ray Photoelectron Spectroscopy (XPS)

X-ray photoelectron spectroscopy, also known under the acronym ESCA (electron spectroscopy for chemical analysis), was developed from the group of Siegbahn at the University of Uppsala in Sweden[12,13]. The method has its basis from the observations of Hertz[14] and Hallwachs[15] who discovered that solids emit electrons when irradiated with photons of certain energy. This observation, also known as the photoelectric effect, forms the basis of all photoelectron spectroscopic methods.

2.1.1 The photoelectric effect

If a solid sample is irradiated with photons of energy hν, an electron in its initial state will be excited. Depending on the photon energy, the electron will leave the solid and can be detected (final state). These electrons can be used to gain information on the original bonding state of the atom from which they originate.

Initial State Effects- Altering the electronic structure of an atom, to a first approximation will lead to a chemical shift ΔE_b of all core levels. Under normal circumstances, these shifts are attributed to initial state effects. Siegbahn et al[16] showed that the E_B for S 1s orbital changes by approximately 8 eV on oxidation from -2 to +6.

Final State Effects - As a result of the loss of an electron an atom is left in an excited and ionised state. The atom in such a state is unstable and would tend to return to its most stable ground state by a process of reorganisation or charge redistribution (relaxation). The relaxation process is two-fold. A fast reorganisation of electron density in (intraatomic) and around (extraatomic) the photoemitting atom occurs simultaneous to the photoemission process. This tends to increase the kinetic energy (and hence lead to an apparent binding energy decrease) because the positive charge left behind by the photoelectron is screened and the outgoing electron (photoelectron) experiences a lower attraction to its parent atom

than would be the case in the absence of this shielding. This is the classical final state effect in XPS, often referred to as core hole screening, shielding, etc. The second relaxation effect is the decay of the core hole. The vacancy in the inner shell which was created by the ejected electron is usually filled by an electron from an orbital of higher energy resulting in the release of energy, either as a fluorescent photon or an Auger electron. Which of the two channels is dominant in this core hole decay process depends strongly on the nuclear charge of the atom. The Auger process is the most dominant for atoms with low atomic numbers, although fluorescence can also play a role in such a process.

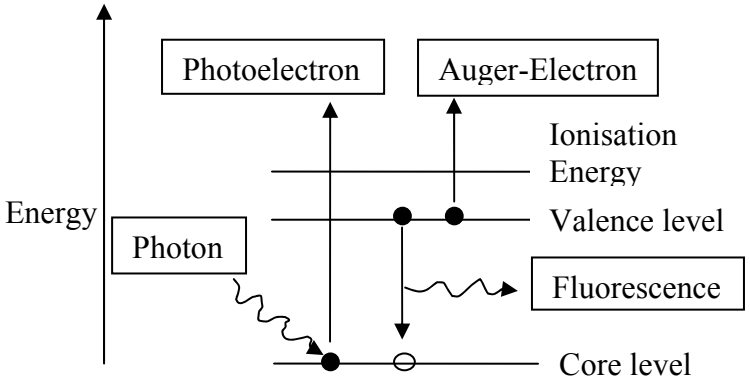

Fig. 2.1: The relaxation mechanism of an excited atom after absorbing an x-ray photon[17].

The advantages of ESCA as compared to related spectroscopic methods are numerous. In addition to the qualitative and quantitative analysis of elements, the method can also be used to distinguish between different chemical states of the same element. A further strength of this method is its almost non-destructive nature. All elements except hydrogen and helium can be investigated by this method. Depth profiling can also be attained with angle resolved XPS (ARXPS) where photoelectrons with different escape depths could be detected.

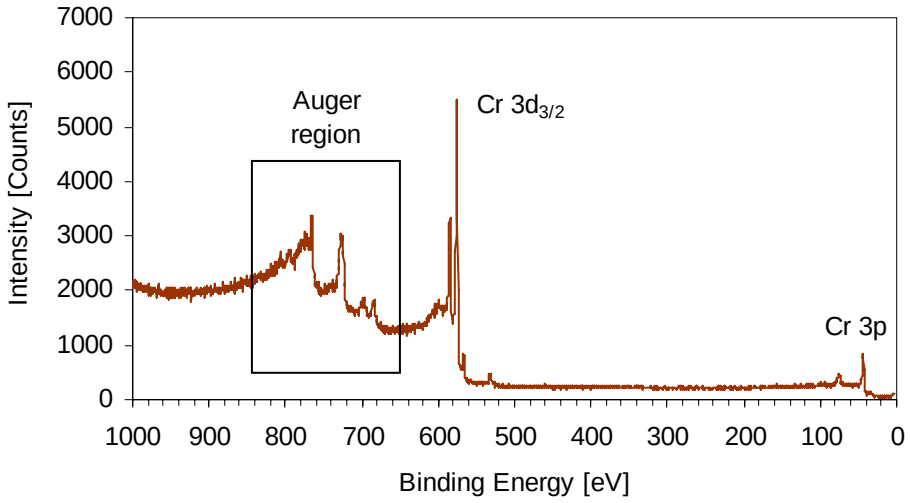

Figure 2.2: XP survey spectrum of a clean Cr(110) single crystal measured with Mg-kα radiation showing both Auger (rectangular box) and photoelectron transitions.

The relevant energy scheme for a photoelectron spectroscopy experiment is illustrated in the figure below:

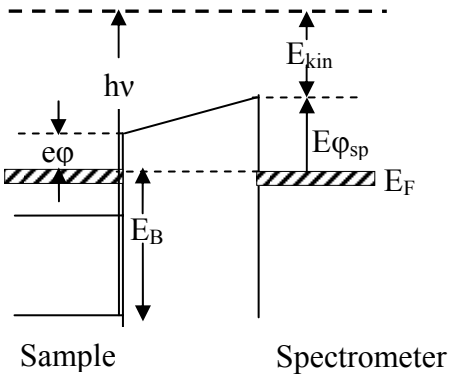

Figure 2.3: Energy diagram for a metal sample in an ESCA experiment. The sample is in electrical contact with the spectrometer[17].

The binding energy E_B of an orbital is expressed mathematically by the modified Einstein equation:

$$E_B = h\nu - E_{kin} - \varphi_{sp} \tag{2.1}$$

φ_{sp} is the work function of the spectrometer, E_B the binding energy of the photoelectron with respect to the Fermi level, E_{kin} the kinetic energy of the photoelectron and hν the

energy of the primary radiation. If on leaving the solid, the emitted electron does not interact with the former in such a way as to cause a change in its original energy and even if the momentum and direction are changed, elastic scattering would have occurred.

The surface sensitivity of ESCA is provided by the relatively small inelastic mean free path (IMFP) of the photoelectron in solids. The ASTM E-42 Committee on Surface Analysis defined the IMFP as the average distance that an electron travels between successive inelastic collisions[18]. This is a simple definition that is commonly accepted. It is however worth mentioning that the electron trajectory between inelastic collisions may not be a straight line because of elastic collisions that an Auger electron or photoelectron may suffer in the solid before being detected. This is a complicating factor in any experimental approach to determine IMFP values. The IMFP is a function of the kinetic energy of the electrons. For most materials, electrons with kinetic energies between 10-1500 eV have IMFP values of several nanometers[19,20].

Energy Scale Calibration - We have seen from fig. 2.3 that the binding energy scale has to be calibrated with respect to the Fermi level. Typically, Au 4f or Cu 2p and 3p lines are used. The lines should be recorded with a narrow sweep width in the range of 5-10 eV, and a pass energy of 25 eV or less or any such energies that are used for high resolution scans. There is no general agreement on accurate values of any standard line energies, but the Au $4f_{7/2}$ at 83.8 eV, Cu $3p_{3/2}$ at 74.9 eV are widely accepted[21]. This consideration is however, valid only for conductors. Semiconductors and insulators require more sophisticated calibration of the BE scale. The Einstein equation for insulators becomes:

$$E_B^V = E_B^F + \varphi_s \cdot e = h\nu - E_K + \varphi_e \cdot e \qquad (2.2)$$

Where E_b is the binding energy and the superscripts “v” and “f” denote that the former is referenced to the vacuum and Fermi levels respectively. φ_s is the sample work function, E_k is the electron kinetic energy and hν is the photon energy.

.

2.1.2 The chemical shift

The creation of a core hole is always associated with relaxation and secondary excitation processes. It is therefore not easy to correlate the measured binding energy values to the ground state properties of an element. The binding energy, B_E of an orbital in the proximity of the nucleus is defined as the difference between the total energy of the ionised final state (N-1) and the ground state (N) of an atom. The chemical shift ΔE_B is defined as the difference between the binding energies of an orbital that exists in different chemical binding states. Mathematically, it is expressed by the relation:

$$\begin{aligned}\Delta E_B &= E_x(N-1) - E_x(N) - \left[E_y(N-1) - E_y(N)\right] \\ &= E_x(N-1) - E_y(N-1) - \left[E_x(N) - E_y(N)\right]\end{aligned} \tag{2.3}$$

where x and y are the chemical binding states, respectively. The chemical shift in a nut-shell is the change in the difference between the total energies of the ionised states and those of the ground states[22].

Complications in the quantum mechanical terms make the exact calculation of the total energies somewhat cumbersome. This allows for approximation methods wherein the summation of different energy terms is involved. Two such approximations, namely the Koopman's and Gauss's theorems will be described in short below:

Koopman's approximation takes the quantum mechanical treatment of an atom according to the Hartree-Fock-method. The orbital energies are calculated with the assumption of a one-electron wave function which are occupied according to the Pauli's exclusion principle. The concept of frozen orbital (ionisation energy is calculated with the assumption that all other non-ionised atoms during the ionisation process remain unaffected) is considered. This concept becomes an approximation for many-electron systems. The total (N-1) system actually reacts to the loss of an electron and goes into a state of lower energy. The energy released in the form of relaxation energy E_{relax} is transferred to the emitted electron leading to a reduction in the binding energy of the latter. Also, relativistic effects (E_{relat}) as well as correlation effects have to be considered. The chemical shift is therefore expressed according to the equation:

$$\Delta E_B = \Delta E_H - \Delta E_{\mathrm{Re}lax} + \Delta E_{korr} + \Delta E_{\mathrm{Re}lat} \quad (2.4)$$

ΔE_H is the Koopman's shift and is considered to be the change in the ground state energy, whilst ΔE_{Relax} is often referred to as the change in the final state enegy. ΔE_{Korr} and ΔE_{Relat} are very small and can be neglected.

The Gauss Model, which is an electrostatic model, is simpler and easier to understand [22]. This method is relative and deals with the energy terms of the free atom. The ionisation energy is dependent on the effective nuclear charge q and the charge distribution (electrostatic Eigenpotential V) around the ionising nucleus. The additional relaxation energy is similar to the one described above. If one considers the two different relaxation mechanisms (atomic, local or R^3) and non-atomic, non-local or R^{ea}, then the following scenarios may arise – the binding energy E_B is correlated to the binding energy of the same orbital in the free atom ($E_{B,Atom}$) assuming point charges according to equation 2.5:

$$E_B = E_{B,Atom} + V + kq - R^{ea} + qR^a \quad (2.5)$$

V is the Madelung's potential with $V = \sum_j \left(q_j / r_j \right)$, q_j is the effective charge q on all other atoms and r_j their respective distances from the ionised atom. R^{ea} stands for extra atomic energy and k is a factor that takes into account the interaction between the nucleus and the valence orbitals[23]. q is the effective nuclear charge of the nucleus in the ground state. R describes the atomic relaxation energy, whilst qR^a describes the gain ($q<0$) or loss ($q>0$) in the atomic relaxation energy of the ion with respect to the free atom. The chemical shift is therefore expressed as[24,25]:

$$\Delta E_B = \Delta V + \Delta kq - \Delta R^{ea} + \Delta qR^a \quad (2.6)$$

Thus according to the Gauss's model, the change in Madelung's potential, the change in the effective nuclear charge and the relaxation energy are the three main factors responsible for the chemical shifts in photoelectron spectroscopy.

2.1.3 Quantitative analysis in XPS

In XPS, it is assumed that the ionisation cross section of a core level is independent of the valence state of the element. The peak intensity is therefore proportional to the number of atoms present in the surface. The peak intensity is the area under the peak after background subtraction. The Shirley method[25,26] of background (background is proportional to the intensity of the emission peak) subtraction is very often employed. This was the method used in the spectral analysis carried out throughout this work. The intensity of the photoelectron lines is proportional to the excitation probability σ, which in turn depends on the photon energy of the primary excitation radiation. The relative ionisation cross sections of many electrons are normally calculated with respect to the C 1s orbital. The ionisation cross section of the Kα radiation of magnesium are available in tables[27,28]. The measured intensity is directly proportional to the intensity of the primary radiation I_0 and the number N_A of the atom A. The transmission properties of the analyser $T(E_A)$ and the sensitivity of the detector D also play an important role in the estimation of intensities. The geometry factor of the excitation $L_A(\gamma_1)$ also depends on the angle between detector and x-ray tube. This factor is equivalent to unity for the magic angle of 54.7° (see section 2.6.4.1). The mean free path of the emitted electrons $\lambda(E_A)$ and the angle of collection of the photoelectrons relative to the surface normal φ are also considered. It is therefore possible to estimate the intensity of a photoelectron line of an element A, coming from a layer dx as follows:

$$dI_a = J_0 D(E) L_A(\gamma_1) \sigma_A N_A T(E_A) \exp\left[-x/(\lambda(E_A)\cos(\varphi)\right] dx \qquad (2.7)$$

The parameters J_0, D(E) and $L_A(\gamma_1)$ are constant for a particular X-ray source, spectrometer and geometry. Integration of equation 2.7 yields:

$$I_a = C\sigma_A N_A T(E_A) \lambda(E_A) \cos(\varphi) \{1 - \exp\left[-x/(\lambda(E_A)\cos(\varphi)\right]\} \qquad (2.8)$$

Assuming the thickness of the layer is ($d >> \lambda$), equation (2.8) simplifies to:

$$I_a = C\sigma_A N_A T(E_A) \lambda(E_A) \cos(\varphi) \qquad (2.9)$$

For very thin layers, equation (2.9) simplifies further to:

$$I_a = C\sigma_A N_A T(E_A) \tag{2.10}$$

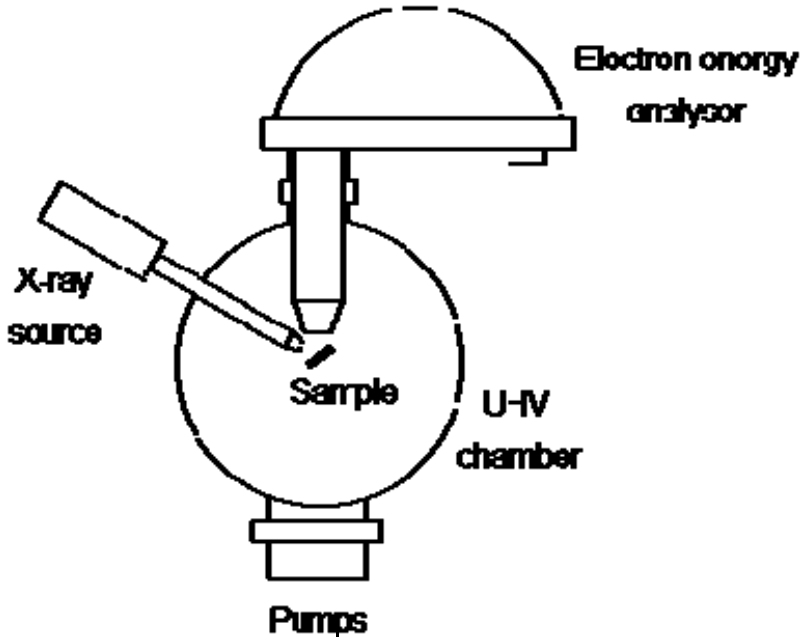

Figure 2.4: Experimental set-up in XPS.

A conventional laboratory XPS experimental set-up is shown in figure 2.4. The photon source is either Mg or Al K_α radiation with energies 1253.6 and 1486.3 eV respectively. The photons are detected with an energy dispersive element of the concentric hemispherical analyser (CHA) type.

2.2 Auger Electron Spectroscopy (AES)

Auger electrons were first observed by Pierre Auger in 1925 whilst irradiating photo plates with x-rays[29], but it was not until some 30 years later that the method became applicable in surface analysis[30]. AES, like XPS, is also based on the irradiation of a solid with a primary beam of energy E_0. Unlike XPS, this source of radiation could either be electrons (electron induced), or photons (X-ray induced).

2.2.1 The Auger process

In this process, outer and inner electronic shells of atoms become ionised and relaxation can occur via two different routes:

a) The core hole could be filled by an electron from a higher energy level of the same atom, and a resultant emission of energy (x-radiation) occurs according to $\Delta E = hv$.
b) The core hole could be filled by an outer electron, giving rise to an energy transfer to a second electron occupying a higher energy level in a radiationless manner. The ejected electron leaves the atom with a characteristic kinetic energy E_K.

It is evident from the figure 2.5 that three processes are in play here – a) the ionisation of an inner shell (K-shell), b) the transition of an outer electron to fill the lower energy hole and c) the energy transfer to a third electron (the Auger electron). Three electronic states participate in the Auger process, but the last two do not necessarily have to be different (e.g. L_1L_1 or L_1L_2) and the kinetic energy of the Auger electron can be written as:

$$E_{kin} = E_1 - E_2 - E_3 \tag{2.11}$$

E_1 denotes the binding energy of the initial core electron prior to ionisation, E_2 that of the electron that fills the core hole and E_3 that of the ejected electron (Auger electron).

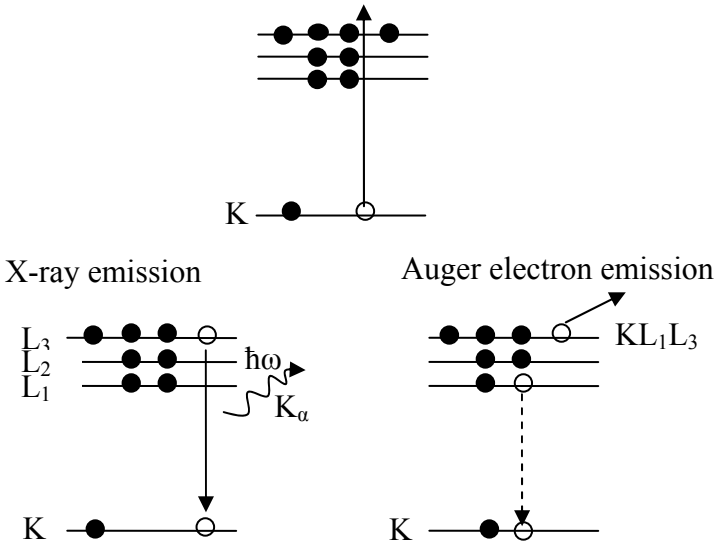

Figure 2.5: Energy-level diagram illustrating two possible filling mechanisms of a K-shell core hole. An x-ray is emitted on the left and an Auger electron with well defined and characteristic kinetic energy is ejected from the L_3 sub-shell on the right[31].

Because the Auger process involves well defined energy levels and because the arrangement of such levels is unique for each atom, AES like XPS is a core level spectroscopy. Figure 2.6 is the survey Auger spectrum of clean Cr(110) single crystal.

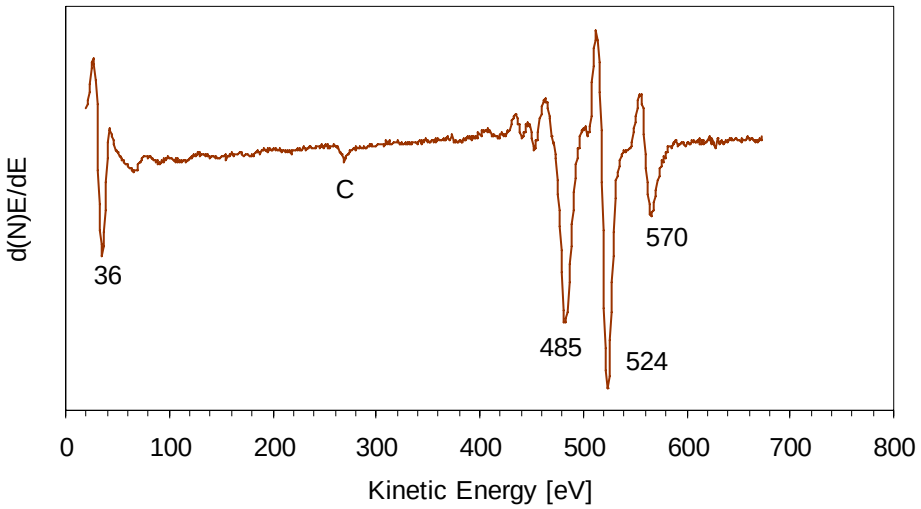

Figure 2.6: Survey Auger spectrum of clean Cr (110) surface showing the most intense transitions. Note that the region marked by the rectangle in fig. 2.2 corresponds to the region between 400 and 600 eV in the figure above.

For atoms with large atomic numbers, there are many different Auger electrons. The capital letters denote the shells, whilst the subscripts to the right of these letters describe the sub-shells involved in the Auger process arranged in ascending order, i.e., in the sequence in which the processes of core hole creation, relaxation and ejection of the Auger electron occurred. A KL_1L_2 transition means that a hole that was created in the K-shell was filled by an electron from the L_1-shell and the Auger electron was ejected from the L_2-shell.

When a surface is irradiated with medium energy electrons, the energy distribution of the back scattered electrons can be divided into three regions. The first and low kinetic energy region is composed mainly of true secondary electrons. At the high energy end, there is a sharp asymmetrical peak depicting elastically reflected electrons. The intermediate region is characterised by a smooth background with small peaks. These peaks are due to Auger electrons. The principal experimental hurdle in AES is therefore to separate these electrons. An effective way to do this is through the application of the electronic-differentiation modulation technique used in combination with a lock-in-amplifier. The experimental set-

up is shown in figure 2.7. A 4-grid LEED optics can be fine-tuned to function as a retarding field analyser (RFA). This is done by applying a negative sweep potential to the second and third grids with the LEED screen acting as an electron collector.

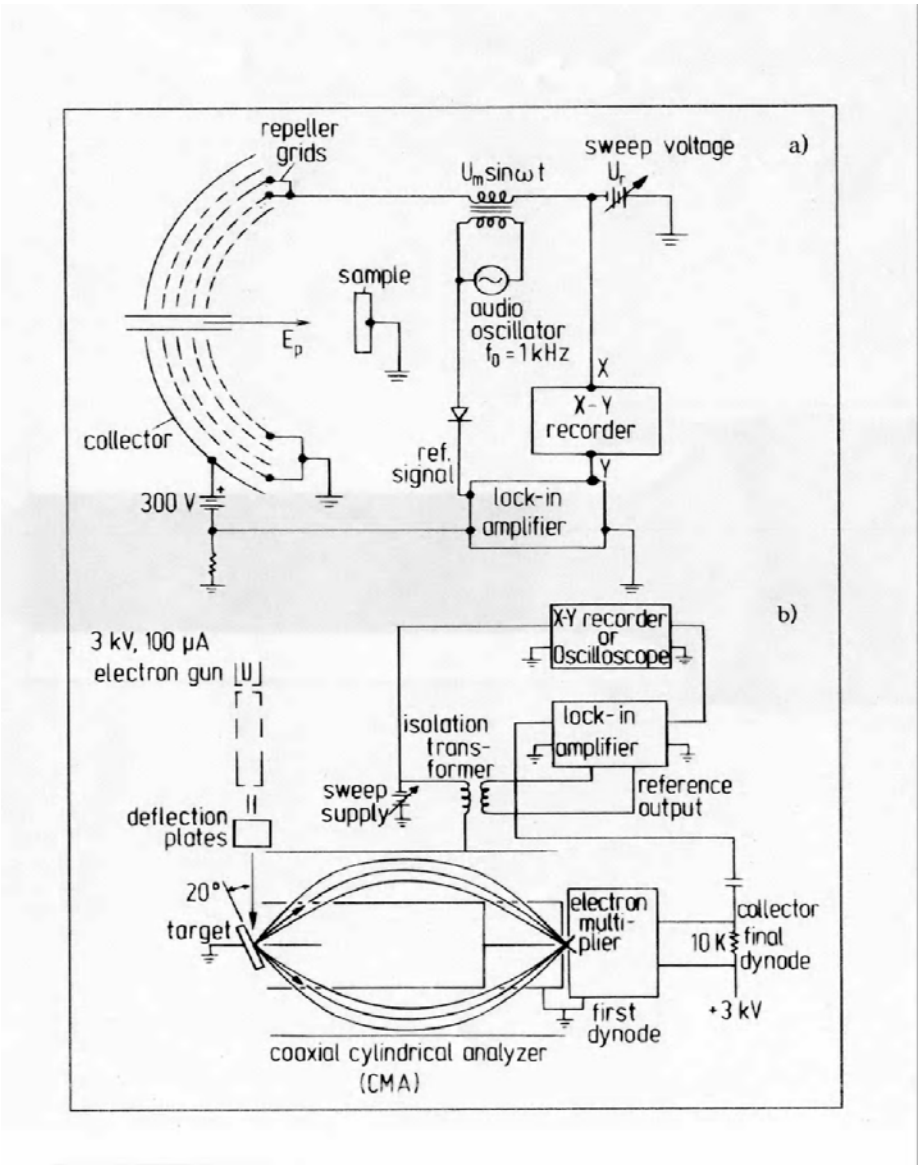

Figure 2.7: Experimental set-up for AES- (a) using the retarding field analyser (RFA) often achieved by a conventional 4-grid LEED optics to obtain differentiated electron-energy distribution dN(E)/dE; (b) using a cylindrical mirror analyser as an energy dispersive element[31].

In the electron differentiation method, the second derivative of the collector electron current, which is proportional to the first derivative of the energy distribution curve [dN(E)/dE], is measured. As a result, electron-induced Auger spectra are presented with the y-axis expressed in the derivative rather than the absolute intensity form. Spectra recorded

using the LEED optics are often of a poor quality due to the large signal to noise ratio. A much more elegant way of solving this problem is the use of the cylindrical mirror analyser (fig. 2.7 b)[31]. Most CMAs contain an integrated electron gun that allows for normal incidence only (note that in figure 2.7 b, the angle of incidence is 20°, the so-called grazing incidence). We used normal incidence in our experiments because of configurational restrictions. The CMA used in this work contained an in-built electron gun with an exit angle of 27°.

2.3 Ion Scattering Spectroscopy (ISS)

Ion scattering spectroscopy (ISS) involves bombarding a surface with a noble gas ion of defined kinetic energy E_0 (e.g. He^+) and then measuring the energy E_i of the back scattered ions. Because every atom interacts differently with the impinging He ions, the kinetic energies of the ions after scattering at a surface will reflect the elemental composition of the surface at which scattering occurs. Most modern electron analysers can be used for this purpose as well. ISS is divided into two separate regions depending on the primary ion energies. These are – low energy ion scattering (LEIS) with energies between 500 - 5 keV and high energy ion scattering (HEISS) or Rutherford back scattering (RBS) in the 100 keV – MeV region. In this work, low energy (0 – 1 keV) was employed. Unlike other deep-probing methods, LEIS has the advantage that it probes only the first atomic layers and therefore can unequivocally help to unravel the surface cocomposition of any material.

A typical LEI spectrum is shown in figure 2.8. The spectrum is that of clean Cr measured at 298 K with a He partial pressure of $2 \cdot 10^{-7}$ mbar and an electron beam energy of 0.5 keV. The small peak around 275 eV is due to oxygen, a species that is always found on bcc surfaces no matter how clean they may be.

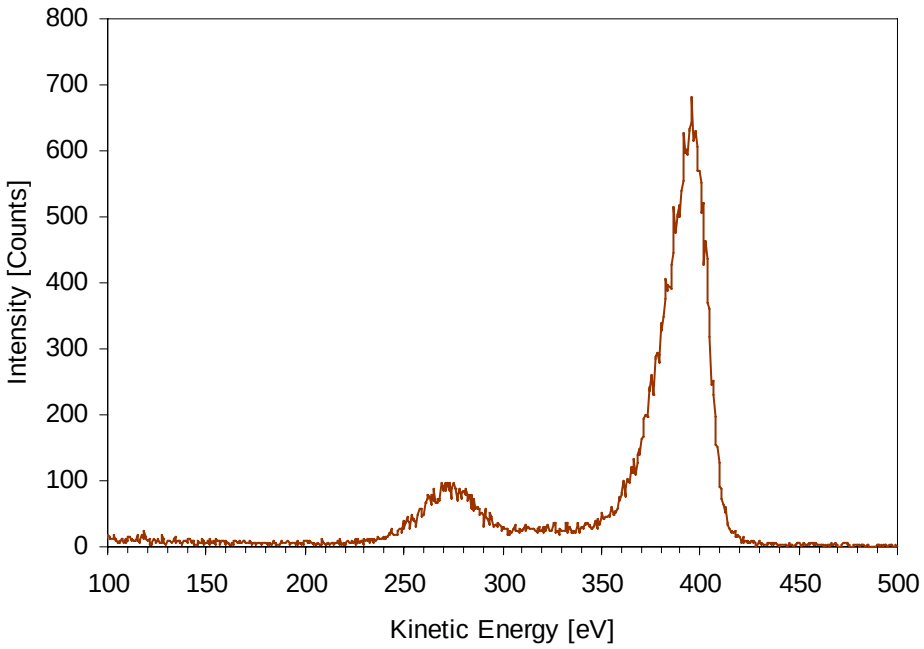

Figure 2.8: LEI Spectrum of clean Cr (110) surface measured at a He partial pressure of $2 \cdot 10^{-7}$ mbar, 0.5 keV.

Low to moderate energy ion scattering is advantageous because of the following reasons[32]:

- Ions are scattered at the surface in simple kinematic two center collisions
- Interaction distance is < 10 Å
- Ions are scattered from a corrugated surface potential
- Interaction time is short < 1 ps
- There is little electronic energy transfer
- Ions are scattered inelastically by simple momentum transfer

2.3.1 Theory of LEIS

From the kinematic theory of elastic collision, the following equations can be formulated from the energy and momentum transfer processes[32]:

Conservation of energy - $$\frac{1}{2}M_1 v_0^2 = \frac{1}{2}M_1 v_1^2 + \frac{1}{2}M_2 v_2^2 \quad (2.12)$$

Conservation of Momentum- $$\| \; M_1 v_0 = M_1 v_1 \cos\theta + M_2 v_2 \cos\phi \quad (2.13)$$

$$\perp 0 = M_1 v_1 \sin\theta - M_2 v_2 \sin\phi \tag{2.14}$$

Square eqn. 2.13: $$\left(M_1 v_0 - M_1 v_1 \cos\theta\right)^2 = {M_2}^2 {v_2}^2 \cos^2\phi \tag{2.15}$$

And 2.14: $${M_1}^2 {v^2}_1 \sin^2\theta = {M_2}^2 {v_2}^2 \sin^2\phi \tag{2.16}$$

Add 2.15 and 2.16: $$\frac{{M_1}^2 {v_1}^2}{{M_2}^2 {v_2}^2} \cdot \sin^2\theta + \frac{\left(M_1 v_0 - M_1 v_1 \cos\theta\right)^2}{{M_2}^2 {v_2}^2} = 1 \tag{2.17}$$

From 2.12: $${v_2}^2 = \frac{M_1}{M_2} {v_0}^2 - \frac{M_1}{M_2} {v_1}^2 \tag{2.18}$$

Subst. in 2.17: $$\frac{{v_1}^2}{{v_0}^2}\left[\frac{M_1}{M_2}\left(\sin^2\theta + \cos^2\theta\right) + 1\right] - \frac{v_1}{v_2} \cdot 2\frac{M_1}{M_2}\cos\theta + \left(\frac{M_1}{M_2} - 1\right) = 0 \tag{2.19}$$

Eqn. 2.19 is a quadratic equation of the type:

$$x^2 + px + q = 0 \rightarrow x_{1,2} = -\frac{p}{2} \pm \sqrt{\frac{p^2}{4} - q}$$

The solution is: $$\frac{v_1}{v_0} = \frac{M_1 \cos\theta \pm \sqrt{{M_2}^2 - {M_1}^2 \sin^2\theta}}{M_1 + M_2} \tag{2.20}$$

$$\boxed{k = \frac{E_1}{E_0} = \left[\frac{M_1 \cos\theta \pm \sqrt{{M_2}^2 - {M_1}^2 \sin^2\theta}}{M_1 + M_2}\right]^2} \tag{2.21}$$

$$k = \frac{\left(\cos\theta \pm \sqrt{A^2 \sin^2\theta}\right)^2}{\left(A+1\right)^2} \tag{2.22}$$

Where $A = \frac{M_2}{M_1}$ (ISS) scattered primary particles. Similarly, for recoils:

$$\frac{E_2}{E_1} = \frac{4M_1 M_2}{\left(M_1 + M_2\right)^2} \cdot \cos^2\phi \tag{2.23}$$

In Summary:

(1) $E_1 = E_0 \cdot k(\theta, A)$ k = kinematic factor (ISS)

(2) $E_2 = E_0 \cdot T(A) \cdot \cos^2 \phi$ $T = \dfrac{4A}{(1+A)^2}$ (Recoil)

For θ = 90°, $\boxed{\dfrac{E_1}{E_0} = \dfrac{M_2 - M_1}{M_2 + M_1}}$ and for θ = 180°, $\dfrac{E_1}{E_0} = \left(\dfrac{M_2 - M_1}{M_2 + M_1}\right)^2$ (2.24)

In this work, the geometry was such that θ is 90°, therefore equation 2.24 was used to estimate the kinetic energy positions of the respective atoms in the surface. With primary He energy of 500 eV, three different energies on the K.E scale at 270, 350 and 390 eV corresponding to oxygen, aluminum and chromium respectively, were detected.

2.4 Low Energy Electron Diffraction (LEED)

The wave theory of electrons was first postulated by De Broglie, but it was not until 1927 that experimental evidence for this theory was supplied by Davisson and Germer who studied the reflection at nickel targets in vacuum[33,34]. That electrons had particulate properties was well established already. The method, which involves bombarding a surface with low energy electrons (20–500 eV) and detecting the elastically backscattered electron waves on a fluorescent screen, is a potent tool in the analysis of well ordered surfaces. Because the wave length of low energy electrons is in the order of magnitude of a few Angstroms, the back scattered electrons could only originate from the surface region of a sample. LEED is therefore the method of preference when information on surface geometries is required.

A much more specialised use of LEED is the I/V (intensity/voltage) method. In I/V analysis, the intensity of a particular spot is measured at different electron energies in increasing order. Such curves, which show intensity maxima and minima as a function of primary electron energy, are then compared to theoretical ones for a particular system, supplying information on the absolute position of the respective scatterers in the elementary cell.

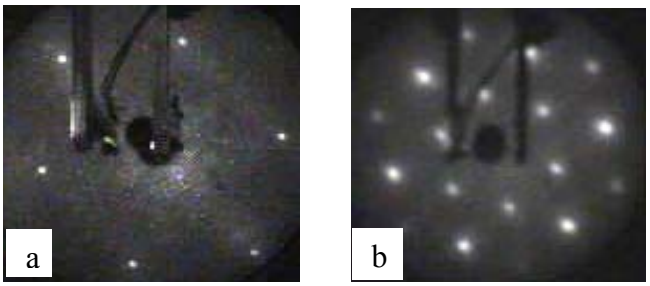

Figure 2.9: LEED patterns of a) Cr(110) and b) Cr_2O_3(0001) recorded at 69 eV respectively.

LEED patterns are described according to the Wood nomenclature[35] which describes the relationship between the adsorbate lattice vectors $(|\vec{b}_1|,|\vec{b}_2|)$ and substrate lattice vectors $(|\vec{a}_1|,|\vec{a}_2|)$ as follows:

$$\left(\frac{\vec{b}_1}{\vec{a}_1} \times \frac{\vec{b}_2}{\vec{a}_2}\right) \tag{2.25}$$

Sometimes an angle is added to the brackets, indicating the angle through which the adsorbate lattice has to be rotated in order that both adsorbate and substrate lattices are commensurate. Other common features of the nomenclature include symmetry elements and number of atoms in the elementary cell, e.g. p(2x2), c(2×1), (1×2)-3H where p is primitive, c is centered and 3H depicts the number of hydrogen atoms per elementary cell[36]. For a detailed treatment of the underlying theory of LEED, the interested reader is referred to the excellent text book by Ertl and Küppers[17].

2.5 X-Ray Absorption Spectroscopy (XAS)

XAS, unlike the low energy electron diffraction method does not require long-range order in a sample as a pre-requisite in order to carry out measurements on that particular sample. XAS, like LEED, could provide useful bulk and surface structure information for solids. XAS can also be applied to liquid samples as was done in this work. In addition, its high sensitivity, i.e. the ability to supply reliable information even of practical catalyst particles and promoter distributions in highly diluted samples with overall concentrations of as low

as 10^{13} atoms/cm^2 makes its application very practical in particular to in-situ measurements in heterogeneous catalysis[31].

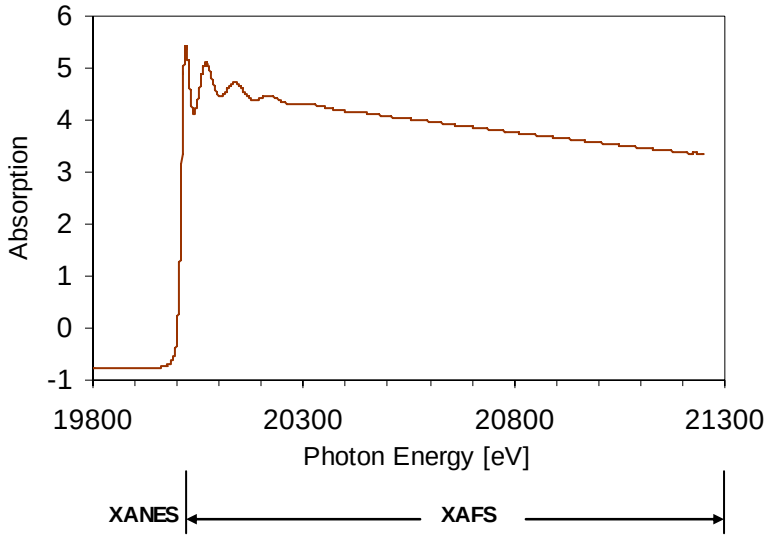

Figure 2.10: Transmission XAFS spectrum of Mo K-edge of a sample of Mo(allyl)$_4$ in pentane measured at HASY Lab, Hamburg.

A typical XAFS spectrum (fig 2.10) contains two distinct regions – a) the near edge region, often referred to as the NEXAFS (near edge x-ray absorption fine structure) or XANES (X-ray absorption near edge structure) and b) the extended x-ray absorption fine structure spectroscopy (EXAFS). In XAFS, type of nearest neighbour, distance of nearest neighbour shells as well as coordination number and geometry (bond angles) can be routinely determined. In addition, XAFS is the routine method used by many scientists, whilst XANES remains a specialist's domain because of the rigorous theoretical input and its corresponding computation involved.

2.5.1 The XAFS process

The primary process in X-ray absorption is the photoionisation of a given atom, whereby depending on the photon energy $\hbar\omega$, excitation of either outer or inner shell electrons is achieved. In XAFS, electrons are ejected from the inner-shell (K-shell). This process requires a minimum amount of energy to occur ($\hbar\omega = E_B$ where E_B is the binding energy of

electrons in the K-shell). For larger photon energies, the energy balance can be expressed thus:

$$E_{kin} = \eta\omega - E_k \tag{2.26}$$

When $\hbar\omega = E_B$, i.e. the first excitation threshold, the so-called K absorption edge is observed in a transmission x-ray spectrum. The larger the atomic number of an element, the larger the photon energy required for K-shell ionisation. For Mo, with atomic number 42, a photon energy of 19,800 eV is needed for K-shell ionisation, whilst Al, with Z = 13, needs about just slightly over 4 keV. In order to produce such high photon energies, synchrotron (electrons emit continuous radiation when accelerated in a circular orbit) radiation is used. The latter has the advantage over conventional laboratory x-ray sources in that it is tunable, continuous and has a high flux density. The problem however, is that synchrotron radiation requires huge material and human input and this sometimes require national and continental cooperation.

2.5.2 XAFS modes

Several modes of data acquisition are employed in XAFS experiments. The intensity of the beam is measured before (I_0) and after (I_t) interaction with matter. The principle obeys the Bear-Lambert's law of dilute solutions.

$$I = I_0 \exp(-\mu d) \tag{2.27}$$

I_0 depicts the intensity of the photons before they interact with a sample of thickness d, while I_1 and I_2 are the intensities after interacting with samples I and 2 respectively. The X-ray intensity is normally measured with the help of ionisation chambers filled with noble gas or N_2. The sample is positioned between two chambers, which are coupled to a normal current measuring device (current measured is proportional to X-ray intensity).

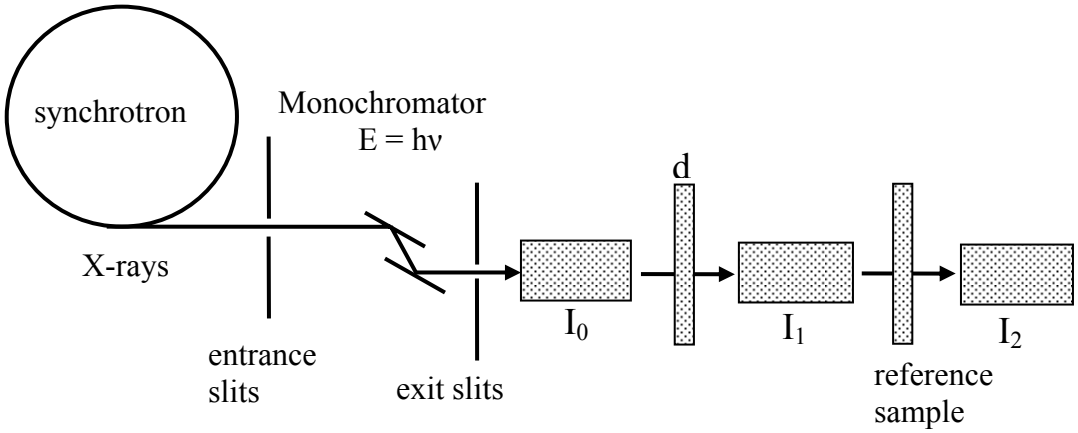

Figure 2.11: XAS as applied in solid state chemistry[37]

The physical quantity obtained with the various techniques is the total inelastic photoabsorption cross section.

The transmission mode is the most commonly used method of XAS data acquisition for it is the simplest in construction. It has a low surface sensitivity and often requires homogeneity of substances in order to supply accurate results. This makes its application unsuitable to catalytic systems. Other methods employed in XAS measurements include the *total electron yield*, *fluorescence yield*, *Auger electron yield* and *ion yield* methods.
In the *total electron yield* method, all detectable electrons leaving the sample surface into vacuum are considered.

The Auger electron yield method lays more emphasis on the Auger electrons only.

In the *ion yield method*, use is made of the fact that the Auger process creates an ion, which relaxes with a specific time constant (τ) to its ground state. If the latter is large enough, the electron could leave the surface and is detectable by a mass spectrometer. This and the Auger method are relatively surface sensitive. As we saw in the figure 2.4, photon absorption can give rise to both the Auger process (which is a radiationless process) as well as fluorescence and depending on the atomic number Z of the element in question, one process predominates.

2.5.3 XAFS function

The XAFS function χ(k), defined as the fractional modulation of the absorption coefficient (μ) caused by the interference, is expressed mathematically as follows :

$$\begin{aligned}\chi(k) &= \frac{\Delta\mu}{\mu_0} \\ &= \sum_j \frac{-N_j \mid f_i(k,\pi) \mid}{k \cdot R_j^2} \cdot e^{-2\sigma_j^2 k^2} \cdot e^{-2\lambda^{-1}k_j} \cdot \sin\left[2kR_j + \delta_j(k)\right] \\ &= \sum_j A_j(k) \cdot \sin\left[2kR_j + \delta(k)\right]\end{aligned} \tag{2.28}$$

Where μ(k) = the oscillatory part of the x-ray absorption coefficient,

$\mu_0(k)$ = the absorption coefficient of an isolated atom,

N_j = the number of scattering atoms at distance R_j,

$f_i(k,\pi)$ = electron scattering amplitude in the backward direction of atom j,

$e^{-2\delta_j^2 k^2}$ = Debye-Waller term accounting for thermal vibrations,

$e^{-2\lambda^{-1}R_j}$ = the damping due to inelastic photoelectron scattering,

λ = electron mean free path,

$\sin[2kR_j + \delta_j(k)]$ = the sinusoidal interference function,

$\delta_j(k)$ = describes the phase shift

2.5.4 Experimental set-up for liquid XAFS investigation of $Mo(C_3H_5)_4$

We performed XAFS measurements of the Mo K-edge using a dilute solution of $Mo(C_3H_5)_4$ in pentane with the simple set-up shown in figure 2.12. The L-shaped stainless steel piece was initially designed for an in-situ catalysis and XAFS cell using metal single crystal surfaces. The six holes (four visible here) are for the purpose of attachment of the XAFS cell. The piece, which measures 80 × 50 × 50 mm contains two long holes (4 mm wide, 40 mm long) 40 mm apart cut into the end resting horizontally on the surface. These holes are for optimum alignment of the piece in the beam. The Teflon tube shown in front

has a volume of 1.4 ml, is 43 mm long and 0.5 mm thick and is closed with a tight-fitting stopper. It was attached to the L-piece using transparent adhesive tape.

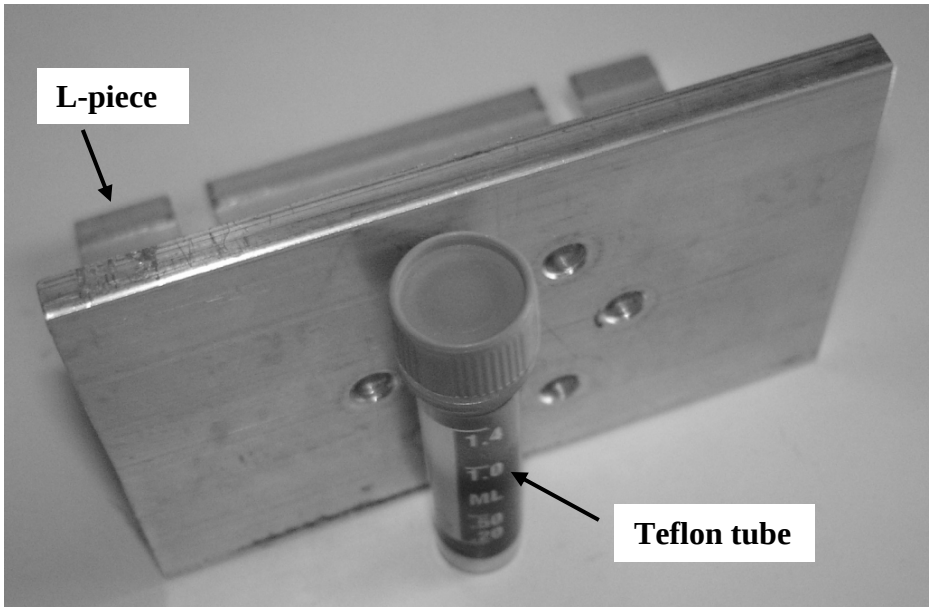

Figure 2.12: Photograph of the sample holder and container used for the measurement of Mo-K edge in a 0.0058 M solution of $Mo(C_3H_5)_4$ in pentane at 300 K. The Teflon tube was fastened to the metal support with a thin transparent adhesive film.

2.6 Nuclear Magnetic Resonance Spectroscopy

This is perhaps the most powerful spectroscopic method available to the chemist today.
The first NMR signals were independently observed by two groups of physicists in 1945. Bloch, Hansen and Packard detected a signal from protons of water at Stanford University, whilst Purcel, Torrey and Pound observed a similar effect from the protons in paraffin wax at Harvard University[38,39].

2.6.1 Theory of NMR

The theoretical basis of NMR stems from the magnetic properties of atomic nuclei. All nuclei possess a nuclear spin and for a particular nucleus, this value could be an integral or half-integral. The proton, for example, which has a nuclear spin I of ½, will have a corresponding magnetic moment μ which will interact with an applied magnetic field. The magnetic moment (μ) can be expressed in units of Bohr magneton as:

$$\mu \propto \frac{e\eta}{2mc} \quad , \qquad \mu = g\frac{e\eta}{2mc}(I) \tag{2.29}$$

The constant m stands for the mass of a proton and e for its charge and g is the so called g factor[40,41]. The magnetic property of a nucleus can also be described by the expression:

$$\gamma = \mu/(I\eta) \tag{2.30}$$

Where γ is referred to as the gyromagnetic ratio. Replacing ge/2mc by γ in equation 2.29 above will reveal that the two equations are identical. This equation shows that a nucleus with a spin quantum number of zero has no magnetic moment. In reality, most elemental isotopes have spin quantum numbers of zero and this includes most of the commonly occuring nuclei (e.g. C^{12}, O^{16}, S^{32}, etc.)

Although there is no comprehensive theory that explains the origin of nuclear spins, some empirical generalisations have been put forward and are summarised in the table below:

Table 2.1 some generalisations for atomic spins[41]

Mass Number	Atomic number	Nuclear Spin
odd	even or odd	½, $^3/_2$, $^5/_2$ (e.g. ^{1}H, ^{17}O)
even	even	0 (e.g. C^{12}, O^{16}, S^{32})
even	odd	1, 2, 3 (e.g. H^2, N^{14})

The number of possible orientations of a magnetically active nucleus in a magnetic field is 2I + 1. A nucleus with a spin I of $^3/_2$ will have five possible orientations ($-^3/_2$, $-^1/_2$, 0, ½, $^3/_2$) which are given by the value of the magnetic quantum number m_I (-I, -I+1, …,I-1, I). This type of splitting of energy levels is called the "nuclear Zeeman splitting"[42,43].

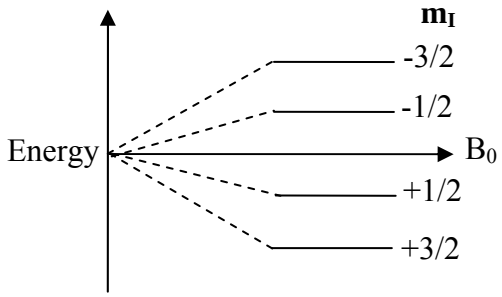

Figure 2.13: Energy levels for a nucleus (I = 3/2) in a magnetic field B.

According to Newton's law, the applied magnetic field will produce an angular acceleration causing the nucleus to precess in the direction of the applied field. The energy difference between any two states is expressed by the equation

$$\Delta E = h\gamma B_0 \frac{1}{2\pi} \tag{2.31}$$

B_0 is the magnitude of the applied static magnetic field, γ is proportionality constant called the gyromagnetic ratio and is constant for each nucleus. This ratio is the probability constant which relates the observation frequency for a particular nucleus to the applied field. The observation frequency is related to γ and B_0 by the relation

$$\nu = \gamma B_0 \frac{1}{2\pi} \text{ or } \omega = \gamma B_0 \tag{2.32}$$

ω is the resonant frequency in radians/sec and ν is the resonant frequency in Hertz. In SI units, B is in Tesla (1 Tesla = 10^4 Gauss), μ in Am^2 and γ is in $rT^{-1}S^{-1}$(r = radian). In obtaining the spectrum of a nucleus, it is either the field or the frequency that may be varied. The magnetic fields obtained in normal laboratories are of the order of 10-100 kG and the resonant frequencies ν of most atoms are in the radio-frequency region (5-400 MHz)[42].

It is the differences in γ between different nuclei that lead to different observation frequencies on a particular spectrometer. The precessional frequency (ω_0) should increase with increase in applied field strength, but there is a limitation to these changes according

to quantum mechanical considerations. Therefore, the angular momentum can have only whole number multiples of h/2π or (ħ) when projected in the direction of H_0. As a result, only a selected number of alignments of nuclei in the applied field are possible. The precessional frequency is also dependent on the magnetogyric ratio γ of the nucleus studied. Mathematically, the relationship is expressed as:

$$\omega_0 = -\gamma H_0 \tag{2.33}$$

ω_0 is known as the "Larmor frequency."

2.6.2 The resonance effect

Now if we consider a nucleus of spin I = ½ , there will be two possible orientations of the nuclear spin ($m_I = \pm 1/2$). The two would be split to energy levels characterised by the nuclear spin quantum number m_I and are seperated by an energy difference ΔE, which is field dependent and very small.

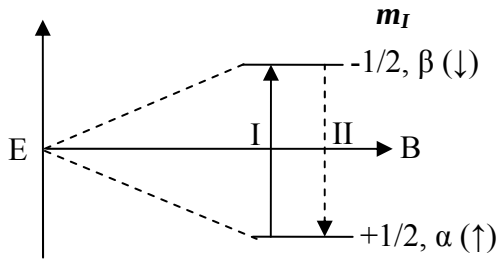

Figure 2.14: Energy levels and transitions for a nucleus (I = ½) in a magnetic field B

The two states exist in thermal equilibrium and only a few nuclei could exist in excess in the lower state. According to the Boltzmann's distribution law, this excess is lower than one nucleus in 10,000. It is this small excess of nuclei that gives rise to the NMR signal. In fig. 2.14, there are two allowed transitions: (a) I → II (absorption) and (b) II → I (induced emission). The coefficients of absorption and emission are equal and as a result there is no net transfer of energy and therefore no NMR signal. This condition does not hold if the sample is in thermal equilibrium for the Boltzmann's distribution law is obeyed. N_α and N_β are the number of spins in the α- and β- states respectively. Because the α- state is more

stable and more populated, there is a net absorption which gives rise to an NMR signal. It is because of this reason that NMR is referred to as a low sensitivity method compared to IR, UV, etc. However, the NMR signal is directly proportional to the number of nuclei producing it[42,43,44].

In the table below is listed some useful nuclei and their magnetic properties:

$$\frac{N_\beta}{N_\alpha} = \exp(-h\nu / kT) \\ = 1 - h\nu / kT (h\nu << kT) \tag{2.34}$$

Table 2.2 Magnetic Properties of some useful nuclei[42]

Isotope	Natural abundance (%)	Spin I (h/2π)	NMR frequency (MHz) for a 23.5kG field	Relative Sensitivity	Electric quadrupole moment
^{1}H	99.98	½	100.0	1.0	_
^{2}H	0.016	1	15.35	0.01	0.227
^{10}B	18.83	3	9.305	0.02	11.1
^{11}B	81.17	3/2	31.17	0.165	3.55
^{13}C	1.108	½	25.19	0.016	_
^{14}N	99.63	1	7.22	0.001	2.0
^{15}N	0.37	½	10.13	0.001	_
^{17}O	0.037	5/2	13.56	0.03	-0.4
^{19}F	100.0	½	94.08	0.83	_
^{27}Al	100.0	5/2	26.06	0.21	14.9
^{29}Si	4.67	½	19.86	0.08	_
^{31}P	100.0	½	40.58	0.07	_
^{33}S	0.74	3/2	7.67	0.0023	-6.4
^{35}Cl	75.5	3/2	9.80	0.0047	-8.0

2.6.3 The chemical shift

We came across the term chemical shift already in section 2.1. By definition, it is the nuclear shielding divided by the applied field[43]. It is measured from a suitable reference

compound which could be a compound in a capillary tube placed in a sample tube (external), or may be added to the sample itself (internal). The solvent peak sometimes also acts as reference. Mathematically, the chemical shift is expressed as

$$\sigma = \frac{(B_{reference} - B_{sample})}{B_{sample}} \times 10^6 \; ppm \tag{2.35}$$

$B_{reference}$ is the magnetic field of the reference nuclei and B_{sample} the field at the sample nuclei. This equation can be re-written as:

$$\sigma = \frac{(\nu_{sample} - \nu_{reference})}{frequency(Hz)} \times 10^6 \tag{2.36}$$

For example in a ^1H spectrum at 60 MHz, two peaks with a separation of 60 Hz are 1 ppm apart. The recommended reference in ^1H NMR is tetramethylsilane $Si(CH_3)_4$. This compound has a σ value of zero which increases in a downfield direction. An alternative nomenclature is the τ-scale, in which TMS is 10 and the scale has a range of 0-10. Comparing the two scales, it is seen that $\sigma = 10-\tau$. Other reference compounds for aqueous solutions include acetone, DMSO, tert-butanol, acetonitril, dioxin, etc.

Because of the spherical symmetry of s-electrons, a circulating electron produces a current which produces a magnetic field at the nucleus. For resonance to take place, it is necessary to increase the applied field to overcome this field. This is the so-called up field or diamagnetic shift. If $B_{ext.}$ is the applied field and B_0 the field at the nucleus, then the nuclear shielding (ΔB) is given by:

$$B_0 = B_{ext} - \Delta B \tag{2.37}$$

Electrons in orbitals other than the s-orbital do not have the spherical symmetry and produce larger magnetic fields at the nucleus and consequently give rise to low-field or paramagnetic shift.

2.6.3.1 The proton

The proton is the only nucleus without a p-electron, and has as a result no paramagnetic term. This accounts for its small range (10 ppm) compared to over 200 ppm for p-electron nuclei. A consequence of this is that the diamagnetic effect can be seen in proton NMR. For example in substituted methanes CH_3X, the electron density around the protons decreases and therefore they resonate at lower fields (increasing σH).
Other factors which affect the proton chemical shift are aromatic ring currents, anisotropic effects, hydrogen bonding shifts, etc.[44,45].

2.6.3.2 Carbon (13)

This has a range of 0-200σ, about 20 times that of the proton. The trend is similar to the proton case with few exceptions (the heavy halogen effect). Going downfield from TMS (σ0), the order of alkanes, olefins and aromatics, ketones and aldehydes is the same in both cases. Furthermore, the effect of substituents in ^{13}C shifts is not confined to the nearest atom, as in proton chemical shift, but that of substituents up to four bonds from the carbon atom must be considered. A set of simple rules for alkanes has been proposed by Grant and Paul[42]. The chemical shift (sigma) of the i^{th} carbon atom in a hydrocarbon chain is given by:

$$\delta_i = -2.6 + 9.1n_\alpha + 9.4_{n\beta} - 2.5_{n\gamma} + 0.3_{n\delta} \qquad (2.38)$$

Nα is the number of carbon atoms bonded directly to the ith carbon, nβ, σ and γ the number of carbon atoms two, three and four bonds removed. The value -2.6 σ is the chemical shift for methane.

2.6.4 Solid state NMR

We have discussed NMR in liquid phase in the last section. Let us now highlight some important features of solid state NMR. The straightforward application of liquid state NMR techniques to the solid state yielded broad lines which are difficult to interpret and

sometimes are not useful at all. The need for solid state NMR arises because some solids are insoluble in a wide range of solvents, others may loose their structural integrity in solution and in most cases it is the solid state structure which is of primary interest as is the case in this work. Solid state NMR also supplements other methods such as x-ray absorption fine structure as has been demonstrated in this work involving the structural elucidation of $Mo(C_3H_5)_4$ using NMR and XAFS. Among the methods for refining solid state spectra are the *magic-angle spinning* (*MAS*), *high-power dipolar decoupling* and *cross-polarisation* (*CP*) techniques. The latter was developed to overcome the problem of low sensitivity in nuclides with low natural abundance (e.g. ^{13}C and ^{29}Si). Each or a combination (e.g. ^{13}C CP MAS) of these techniques enhances spectral properties comparable to liquid NMR spectra. However, the very small range of transition frequencies of the ^{1}H nucleus makes it very difficult to achieve good resolution in most cases[40,41,46].

2.6.4.1 Removal of line broadening from solid spectra

Magic angle spinning is the method for averaging spin interactions and chemical shift anisotropy in solids. In liquids, this effect is averaged to zero because of the rapid isotropic motion. MAS normally involves rapid spinning of the sample about its axis at a specific angle to the applied field. In solids, the two sources of broadening (dipole splitting and CSA) contain an angular dependence of the form $3\cos^2\theta-1$. The essential features of this technique originated from Andrew et al[47], Lowe[48] and Kessemeier and Norberg[49]. This angle (54.73°) is the angle, for which a spinning solid sample produces the same isotropic chemical shifts as does the random motion in liquids. MAS has become so widespread and well-developed that a thorough discussion is beyond the scope of this work.

High-power dipolar decoupling basically involves masking or eliminating the heteronuclear dipolar coupling with the system of abundant spins. Rare spins are normally ^{29}Si, ^{13}C and ^{15}N and abundant spins are mostly protons. Dipolar coupling of ^{13}C to ^{1}H for example can be removed by this method. For detailed account of this technique, see the excellent work by Mehring[46].

Cross polarisation on the other hand involves enhancement of the NMR signal of low sensitivity nuclei by altering population distributions. In this method, which is otherwise

called polarisation transfer, spin-spin coupling is used to transfer the population characteristics of high γ-nuclei (e.g. ^{1}H) to low γ-nuclei (e.g. ^{13}C) by applying so-called polarisation pulses.

2.7 Ultra Violet Photoelectron Spectroscopy (UPS)

The ultra violet photoelectron spectroscopic method is used mainly for the study of the valence electron density of states. The photon source is either a vacuum UV-source (VUV) produced in conventional laboratories with the aid of commercial noble gas discharge lamps, or synchrotron radiation. The VUV discharge covers a range of 10 to 50 eV photon energy with He I and He II excitation lines at 21.22 and 40.8 eV being the usual noble gas lines, respectively, used in the experiment. In the low VUV range (< 20 eV and especially < 12 eV photon energy), the shape and structure of the excitation photoelectron spectra strongly depend on the impinging photons. For VUV photon energies in the range 20 to 40 eV, s-like valence electron structures are suppressed compared to p-like orbitals. At 40 eV and higher, d-like structures are generated with a higher probability[50]. UV photoelectron spectra could therefore, be used for a comparison with band structure calculations and in comparison with XPS, provides some additional fingerprint information in surface chemical analysis.

The innovation of UPS was made at the Imperial College London in the early 60s[51,52] and has until now been recognised as an especially unambiguous method for the study of the molecular electronic structures of substances in the vapour state[53,54]. The energy relationship is similar to XPS where the photoelectric effect is the underlying principle and is expressed by the relation:

$$E = h\nu - I_i - \Delta E_{vib} - \Delta E_{rot} \qquad (2.39)$$

where hv is the energy of a quantum of radiation from a monochromatic source. E is the kinetic energy of the photoelectron and I_i the ionisation energy of the orbital from which the photoelectron is expelled and is expressed relative to the Fermi level. ΔE_{vib} and ΔE_{rot} are the vibrational and rotational energy changes upon ionisation, respectively. The figure

below is the UV photoelectron spectrum of a clean Cr sample measured with He I excitation line at 21.22 eV[53,54]. In UPS neither vibrations nor rotations can be excited.

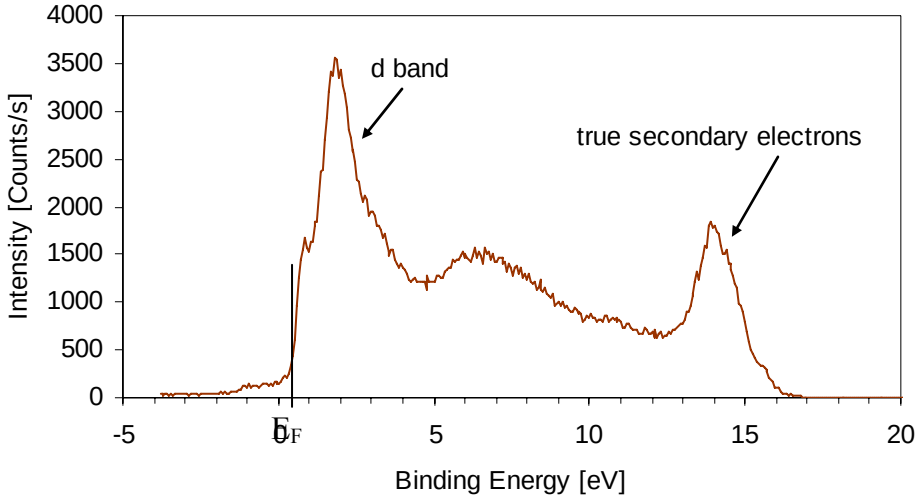

Figure 2.15: He I UP spectrum of Cr(110) measured at 100 mA emission current and He partial pressure of $5 \cdot 10^{-1}$ mbar in the first pumping stage.

2.8 Inductively Coupled Plasma Mass Spectroscopy (ICP-MS)

The inductively coupled plasma mass spectroscopic method is a powerful tool in trace (ppm-ppb) and ultra trace (ppb-ppt) analysis of elements. Plasma is defined as a gas consisting of ions, electrons, and neutral particles[55]. The behavior of the gas is dominated by the electromagnetic interaction between the charged particles. In ICP-MS, the plasma is formed from Argon gas. The plasma is used to atomise and ionise the elements in a sample. This ability to atomise almost any thing from ceramics to glass and gravestones makes this method the method of choice in archeometry. The resulting ions are then passed through a series of apertures (cones) into the high vacuum analyser. The isotopes of the elements are identified by their mass-to-charge ratio (*m/e*) and the intensity of a specific peak in the mass spectrum is proportional to the amount of that isotope (element) in the original sample.

2.8.1 The plasma[55,56,57]

The inductively-coupled plasma is a very aggressive ion source. Because the source operates at temperatures around 7000 K, virtually all molecules in a sample are broken up into their component atoms. In ICP, a radio frequency (RF) signal is fed into a tightly wound, water-cooled coil where it generates an intense magnetic field. In the center of this coil is a specially made glass or quartz plasma torch where the plasma is formed. The plasma is generated in the argon gas by "seeding" the argon with a spark from a Tesla unit (similar to that used on a car spark plug). When the spark passes through the argon gas some of the argon atoms are ionised and the resulting cations and electrons are accelerated toward the magnetic field of the RF coil. Through a series of inelastic collisions between the charged (cations and electrons) particles and neutral argon atoms, stable high temperature plasma is generated. The concentrations of electrons, cations and neutral species in the plasma very quickly reaches equilibrium, after which the plasma will remain 'lit' as long as the RF field is maintained and there is a constant supply of argon gas into the plasma.

The plasma torch is designed in such a way as to allow a sample to be directly injected into the heart of the plasma. The sample consists of a fine aerosol, which can come from any number of sources including, but not limited to, nebulised liquids and ablated solids. As the sample aerosol passes through the plasma, it collides with free electrons, argon cations and neutral Argon atoms. Consequently, any molecules initially present in the aerosol are quickly and completely broken down to charged atoms. These are usually in the univalent (M^+) state although a few divalent (M^{++}) states are also formed. Some of these charged atoms will recombine with other species in the plasma to create both stable and meta-stable molecular species (*e.g.* MAr^+, M_2^+, MO^+, etc.). Many of these molecular species will be positively charged and will also be transmitted into the mass analyser along with the charged atoms (M^+ and M^{++}).

2.8.2 Sampling the ions

A special set of metal cones and ion-focusing elements are used to extract the charged atoms from the plasma, which works at atmospheric pressure, into the mass analyser which

operates at a pressure of 1 x 10^{-7} mbar. The tongue of the plasma is placed across the tip of a water-cooled nickel sampler cone. At the tip of the sampler cone is a small hole that opens into the mass spectrometer.

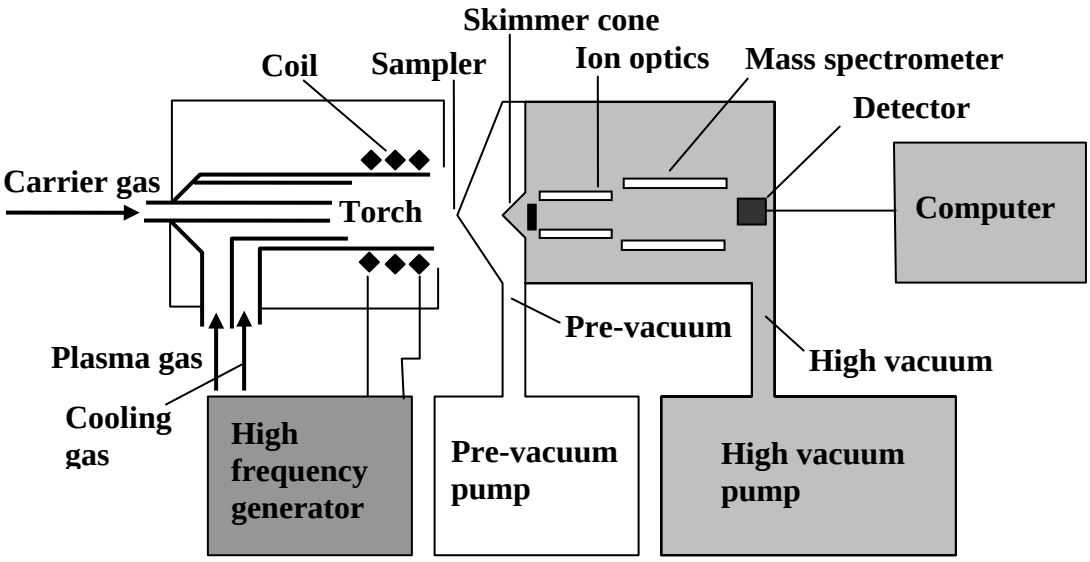

Figure 2.16: Experimental set-up in ICP-MS showing the different compartments[56]

The space behind the sampler cone, the expansion chamber, is evacuated to a pressure of around 1 – 1.5 mbar. The jet of gases passing through the sampler exceeds the speed of sound and creates a conical shock wave, which terminates at a Mach disk as the gases slow down. The inside of this shock wave is known as the zone of silence. The distance from the sampler cone to the Mach disk is proportional to the ratio of the pressure in the expansion chamber and the atmospheric pressure in the plasma. The expansion chamber terminates with another cone known as the skimmer cone. It is situated such that its orifice is located within the zone of silence. Behind the skimmer cone is the mass spectrometer, which is maintained at a pressure of <2x10^{-7} mbar. The ions that successfully pass through the skimmer cone orifice are first accelerated by a high voltage potential gradient and are then passed through a series of focus lenses into the mass analyser. The cones and expansion chamber are often collectively referred to as the interface to the mass spectrometer.

2.9 The Ultra High Vacuum Systems (UHV)

Two different UHV chambers were used during this work. The first one, where AES and LEED investigations were carried out, is a simpler and single compartment chamber whilst the second one, which comprises XPS, LEIS, UPS, a high pressure cell and a transfer rod connecting all components of the vacuum system is much more complex.

2.9.1 The AES and LEED chamber

The AES and LEED experiments were carried out in an ultra high vacuum chamber having a base pressure of 2×10^{-10} mbar, measured by Bayard-Alpert ionisation gauges. The chamber was fitted with a four-grid electron optics for LEED, a cylindrical mirror analyser (Varian) for AES, and with a quadrupole mass spectrometer (Balzers).

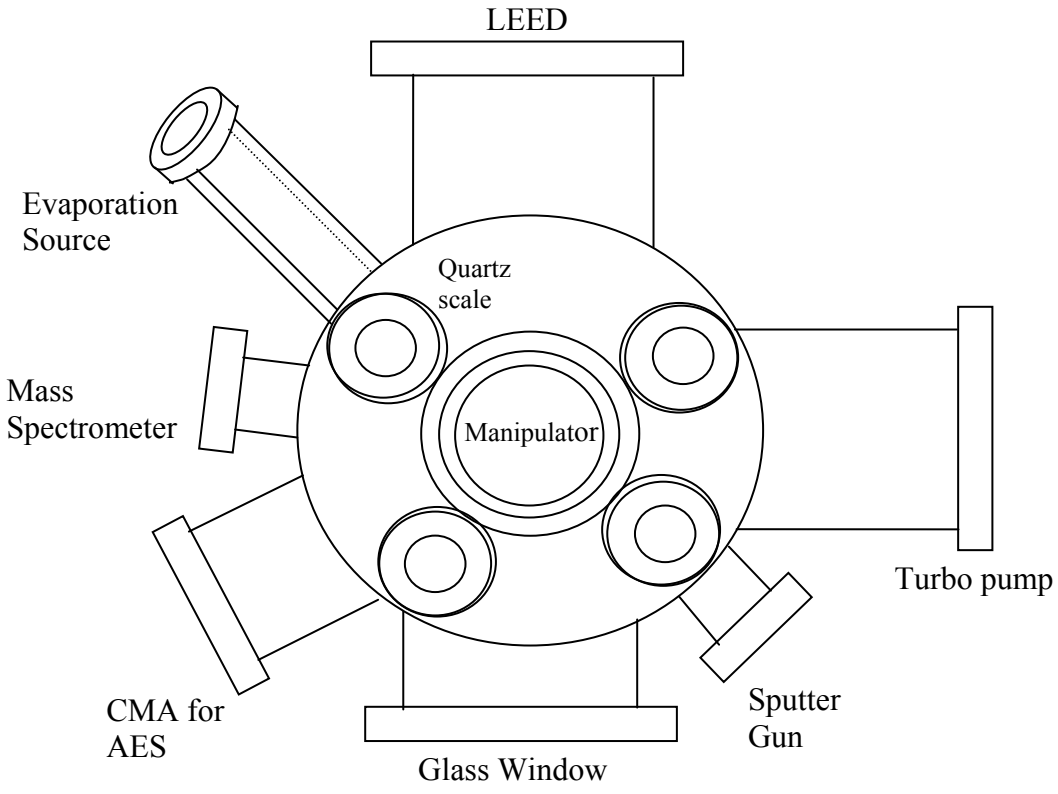

Figure 2.17: Schematic view of the LEED and AES UHV chamber.

In addition, it is also fitted with the usual UHV auxiliaries like a mass spectrometer, a sputter gun, a vertical sample manipulator, and several valves for controlled dosing of several gases as well as a mechanism that allows for sample holding and resistive heating. This chamber contained only one unit where both sample cleaning and analysis were carried out. A detailed diagram of the chamber is shown in figure 2.17:

2.9.2 The XPS, LEIS and UPS chamber

This chamber contains an XPS unit (x-ray source, electron analyser), LEIS, UPS and normal auxiliaries like sputter gun (Leybold), quadrupole mass spectrometer (Balzers), gas dosage valves etc. The most important feature of this chamber is, however, that both analysis and preparation chambers are separate entities connected by a transfer rod that allows for holding and heating the sample resistively.

This transfer rod facilitates the transfer of the sample from one partition to the other without any significant loss of vacuum. It also allows for rotation (360°) of the sample about its horizontal axis to the nearest degree. In addition, there are the two high pressure units with the first one fitted with gas in- and outlets and the second one fitted at the top with a transparent glass window. The latter is also equipped with gas in- and outlets and provides access to the sample. In other words, this is the room that allows for mounting the heating and thermocouple wires. The transfer rod can also be cooled with liquid nitrogen. The vacuum plan of the system is shown in the scheme in figure 2.18. In the figure, the analysis chamber, the preparation chamber, the high pressure chamber for catalysis, the high pressure section for wet chemical/electrochemical reactions and the manipulator are shown. In addition, the pump and valve network, the gas introduction system as well as the network for spectroscopic and cleaning equipments are also presented.

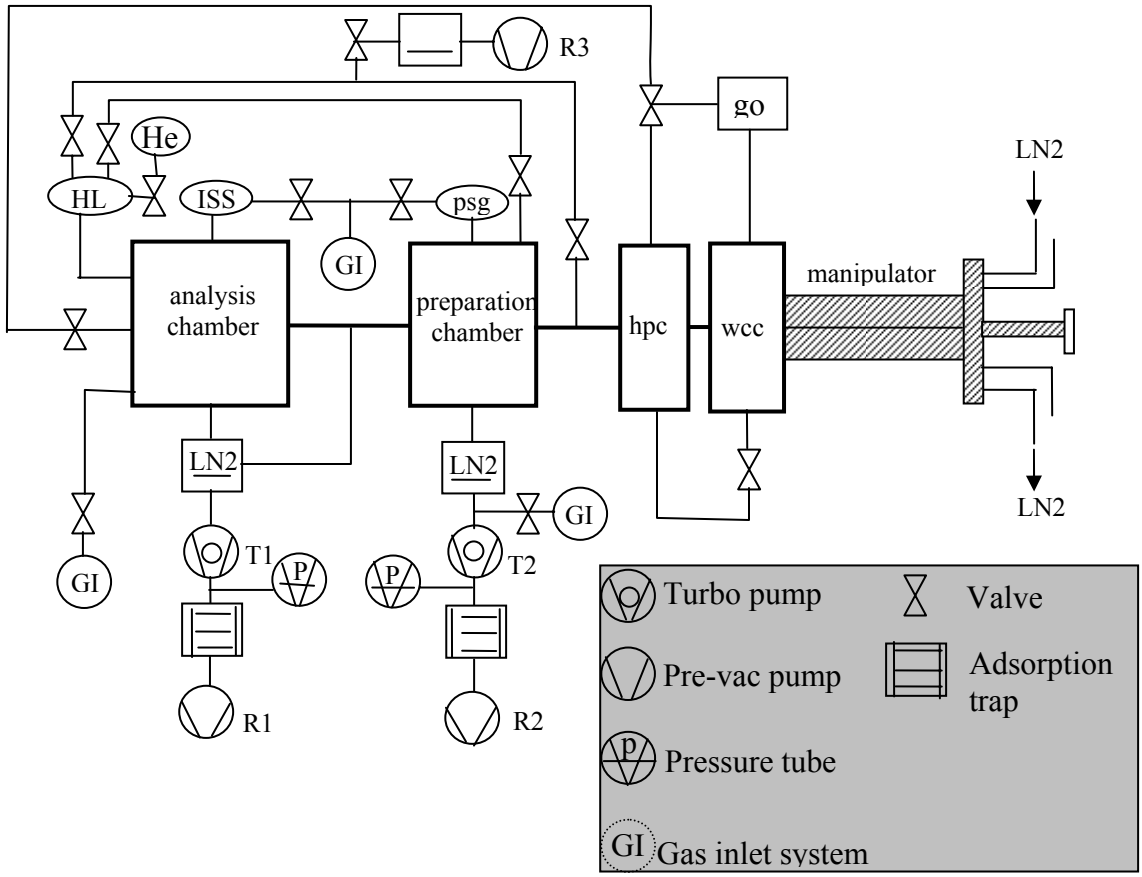

Wcc = wet chemical cell; hpc = high pressure chamber; He = Helium source for the UV lamp; HL = helium lamp; psg = Penning sputter gun, go = gas outlet, ISS = electron gun for ion scattering spectroscopy.

Figure 2.18: Flow diagram of the second UHV chamber used for the wet chemistry as well as XPS, LEIS, UPS and TID measurements.

2.9.2.1 The transfer rod

The transfer rod is a commercially built one (IGT Essen). It has six insulated feedthroughs for sample mounting (4) with thin wires (Ta, 0.25 mm) and the remaining two for measuring the thermo voltage through the Ni/CrNi thermocouple wires. The set- up is shown in the figure below: The main transfer rod is hollow at the point where the crystal is mounted. The hollow nature allows for feedthroughs for cooling, heating and temperature measurements.

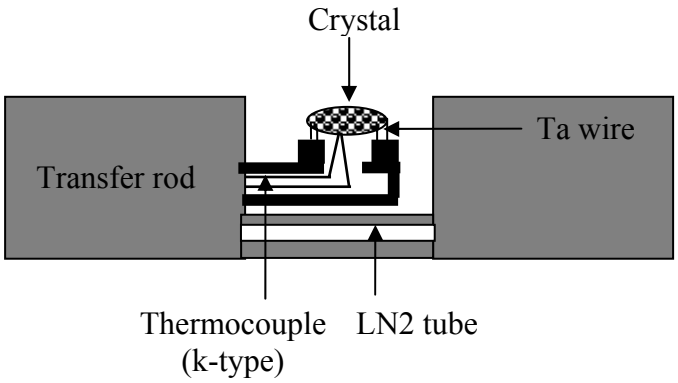

Figure 2.19: Cross section of the transfer rod showing the crystal mount and thermocouple. Note that the space above can be sealed off with a plexi glass window and flushed with gas.

2.9.2.2 The wet chemical cell

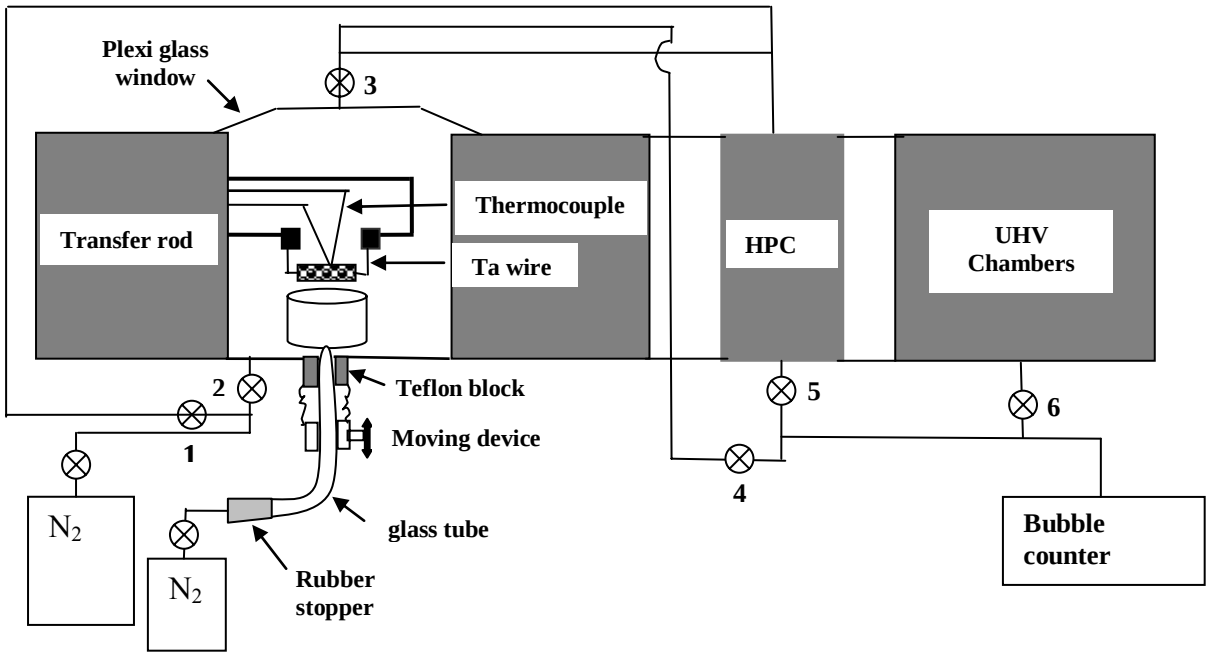

Figure 2.20: Sketch of the UHV transfer system showing the high pressure chamber and glass cell where wet chemical reactions were carried out.

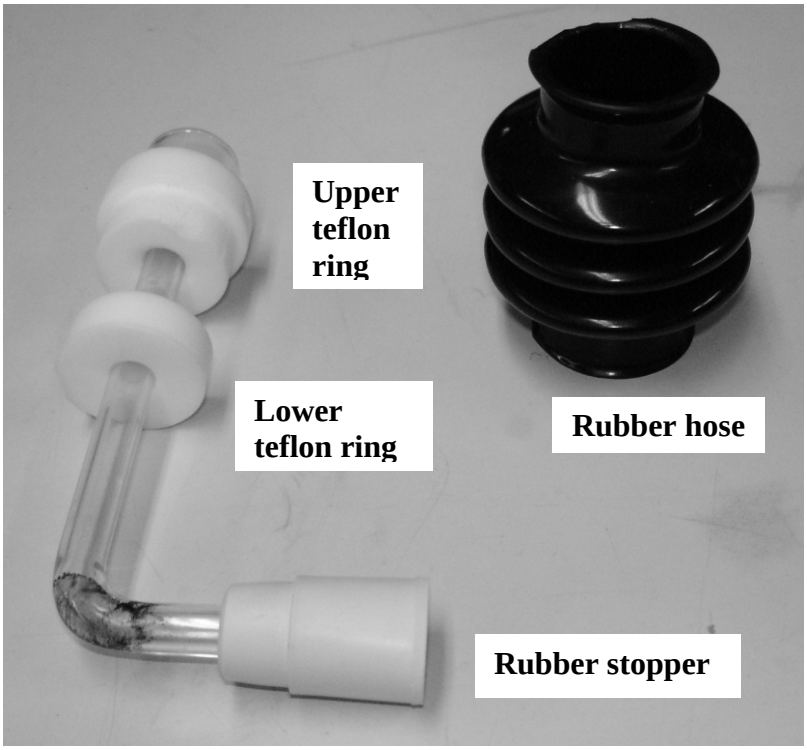

Figure 2.21: Photograph of the main components of the glass cell. The rubber hose was attached between the upper and lower Teflon rings to rid the enclosed space of air.

The upper end of the glass tube has a diameter of 17 mm, spacious enough to accommodate the crystal. The lower end is sealed off with a rubber stopper which is suitable for introducing the sample through injection with a thin needle. The stoppered tube has volume of 6 ml.

In the photograph (2.22), the section of the manipulator system that was constructed for the wet chemical reactions is shown. Valves 1 and 2 are for gas introduction into the system, while 3 and 4 are outlet valves. The glass cell and moving device are visible below the plexi glass window.

With the help of the valves, the space enclosed by the plexi glass window and the upper teflon ring of the glass tube can be flushed with the appropriate gas prior to and during the reaction. A small syringe mounted on the open end of a rubber tube from a gas bottle with a pressure regulator can be used to pierce this rubber without spillage of fluids or ventilation of the system, hence making it possible for the glass tube to be flushed separately with gas.

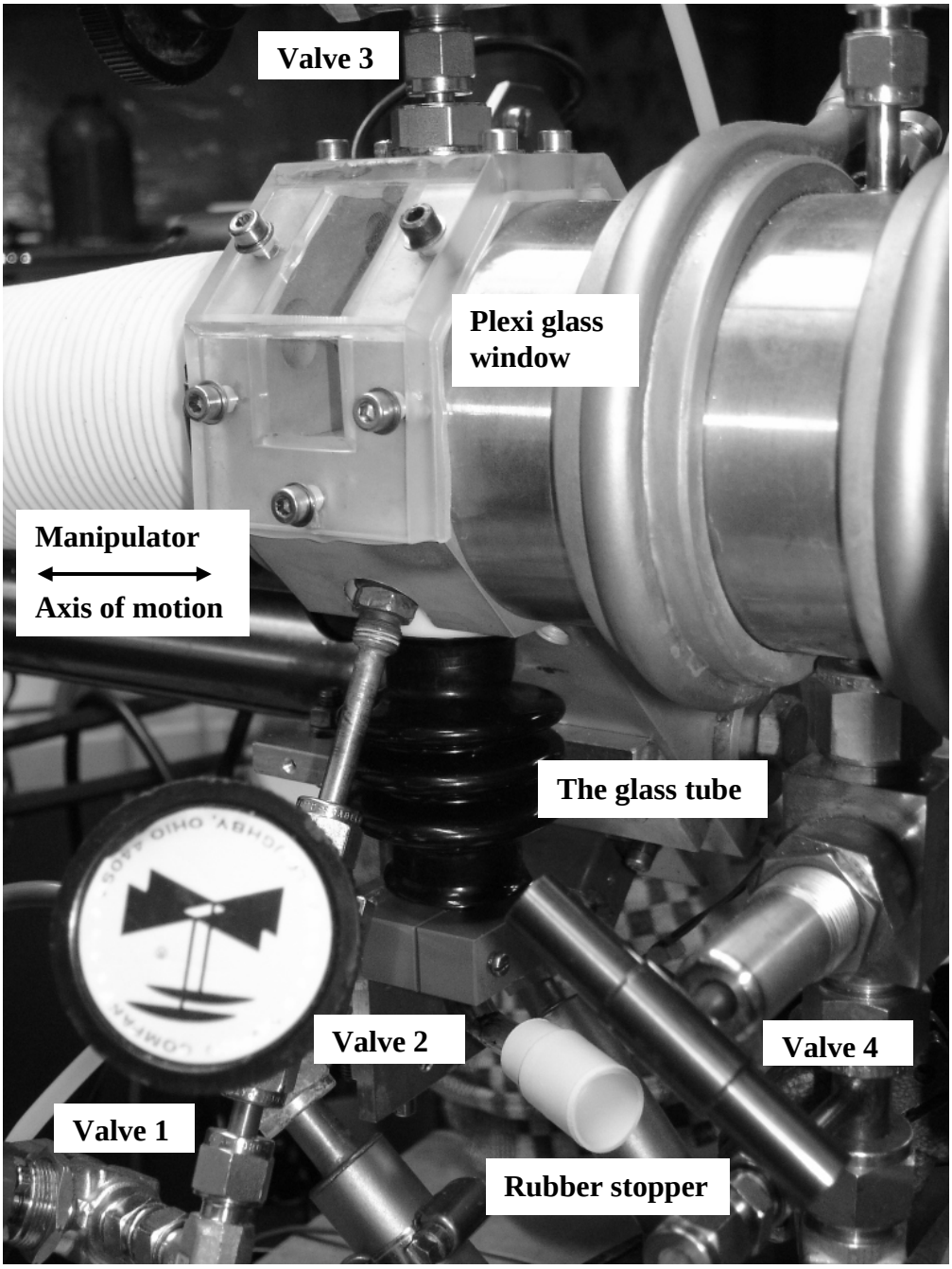

Figure 2.22: Photograph of a section of the manipulator with the high pressure cell, mounted glass tube and valve system.

The plexi glass section is now magnified in the photograph (fig. 2.23) to highlight the crystal and crystal mount on the manipulator rod. The crystal sits in the middle of the rod in a hollow section supported by four Ta wires. The space enclosed by the window is sealed off with a glass sheet and a thick silicone gasket with the aid of sixteen screws.

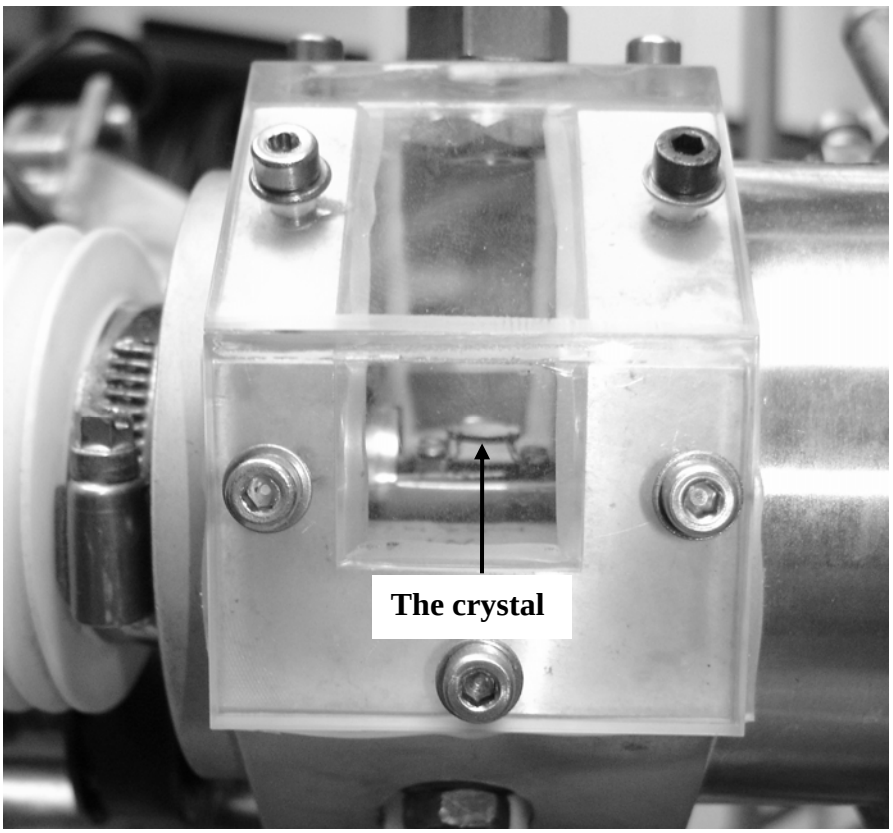

Figure 2.23: A photograph of the plexi glass window showing the crystal mount and the manipulator rod with the crystal held in place by four Ta wires.

The wet chemical reaction between the single crystal surface (Al_2O_3) and $Mo(C_3H_5)_4$ in pentane was achieved by bringing the crystal to the position shown in the figure (2.23), while at the same time the glass tube is filled with a solution of the complex and the whole array is flushed with an inert gas for a few minutes. Eventually, the crystal is rotated through 180° so that it hangs upside down. The glass tube is then moved slowly upwards until the liquid just about wets the surface of the crystal. After a few seconds of contact, the crystal is turned around again and driven into the first pumping stage and finally into the analysis chamber where XPS, UPS and MS investigations of the surface are carried out. After a routine transfer process, the pressure increase in the chamber is about two orders of magnitude.

The pressure increase in the analysis chamber depended heavily on the time the crystal spent in the pre-pumping stages.

2.10 The Single Crystal and Al-source

The sample is a Cr(110) single crystal polished on one side with a nominal miscut of 0.5° with a diameter of 10 mm and a thickness of 1 mm. The crystal was attached between two ends of an L-shaped manipulator by four 0.2 mm thick tungsten wires inserted into four holes drilled into its two opposite ends. Resistive heating of the sample was achieved by applying a current of 10-20 A to the tungsten wires. Temperatures up to 1100 K were achievable by this setup. The sample temperature was monitored by a Ni/CrNi thermocouple (0.2 mm thick) spot welded to the side of the crystal.

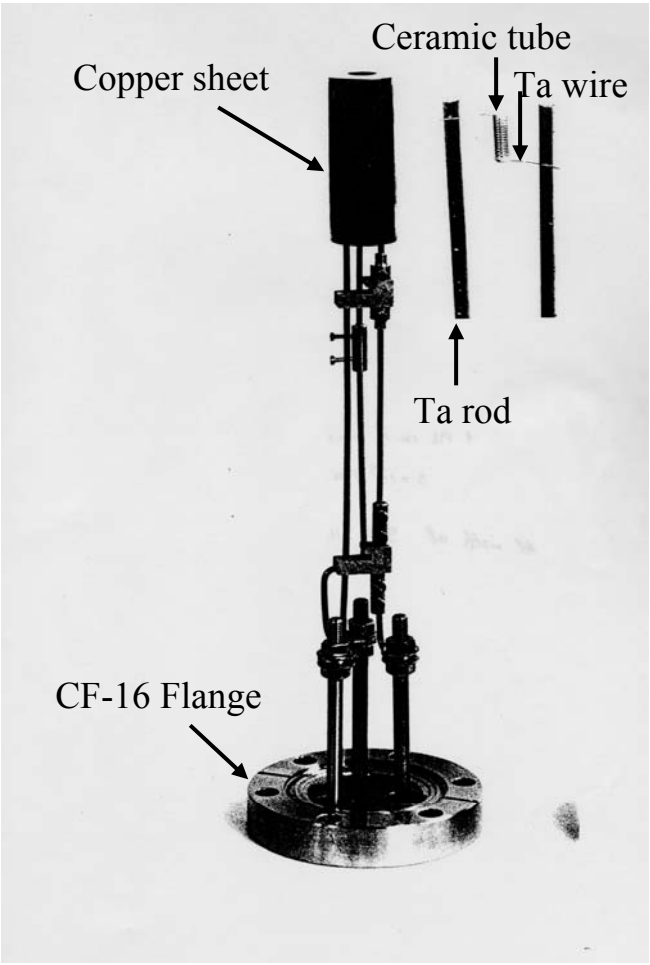

Figure 2.24: Al source built after D. Wytenburg[58]

The Al-source was constructed according to the model of Wytenburg (PhD thesis, Cambridge, 1992)[58]. Al wire was stuffed into a small (2 mm in diameter, 15 mm long)

ceramic tube around which tantalum wire was wound. The free ends of these wires were spot-welded to the top ends of two stainless steel rods whose other ends were mounted on a CF-16 flange. The evaporator was capable of producing a steady and reproducible flux of Al under the operating conditions and had a low heat capacity.

All gases used (Messer Griesheim) (O_2, He, Ar) were of analytical grade Griesheim GmbH, 99.99%) and were dosed through variable leak valves. Aluminium wire of high purity (99.98 %, Advent Research Materials, Ltd., UK) was used for evaporation.

2.11 The XAFS Cell

The cell is composed of three main parts: the blank CF-16 flange, the teflon block (holds the crystal) and the teflon cap (fig. 2.27). The flange, which has a diameter of 33 mm and a thickness of 7 mm, forms the basic component. Three holes, drilled through the sides in a triangular arrangement open through the center of the flange. Six additional holes drilled in a hexagonal array into the sides enhance the encapsulation of the teflon block (and crystal) with the help of the teflon cap. The cap, which has the same diameter as the flange itself, sits perfectly on top of the former. The top section of the cap has a diameter of 16 mm and is less than 0.4 mm thick. This allows for more than 80% transmittance of radiation. The block, which sits coaxially in the middle of the flange, is 10 mm high and 15 mm in diameter. At the top of the block is a groove about 11 mm in diameter and 0.6 mm deep. The crystal sits in this groove and is held in place with the aid of three screws so that the assembled array can be rotated through 180° without the crystal falling off. The block is fastened to the metal base with the help of a hole drilled through it to the center of the flange. On the edges of the block are found six holes, three through which the crystal can be held in place with screws and three for evacuating the unit as well as flushing with gas. Three small pipes welded to the sides of the flange with swage locks make it possible for the complete setup to be connected to a vacuum or gas line. The rubber gasket provides an air-tight sealing between the cap and metal piece while the six long screws and nuts make it possible for the unit (see fig. 2.25) to be mounted on a metal holder.

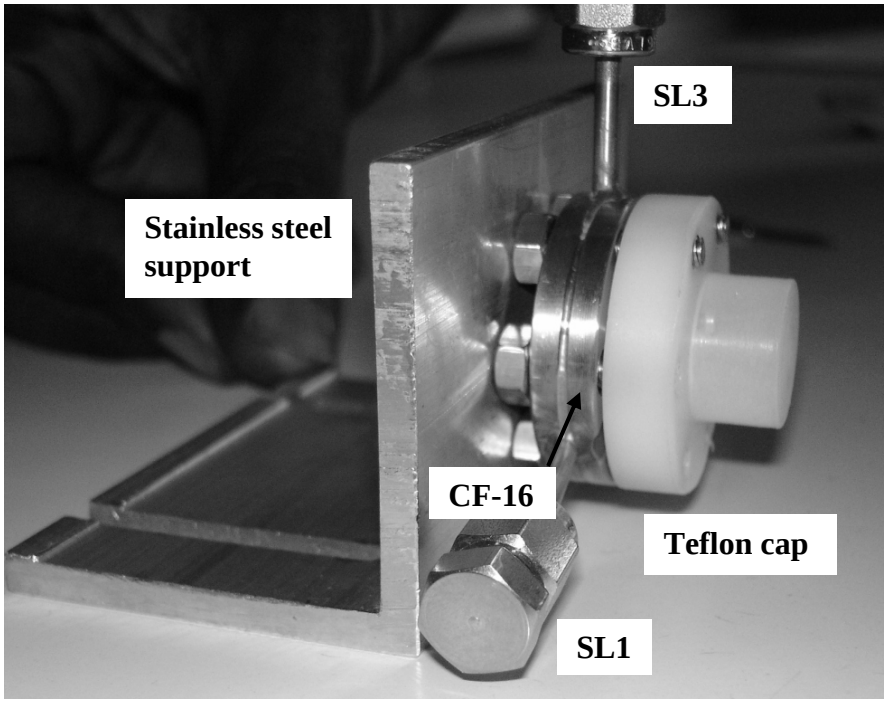

SL = Swage lock
Figure 2.25: Side view of the XAFS and catalysis cell

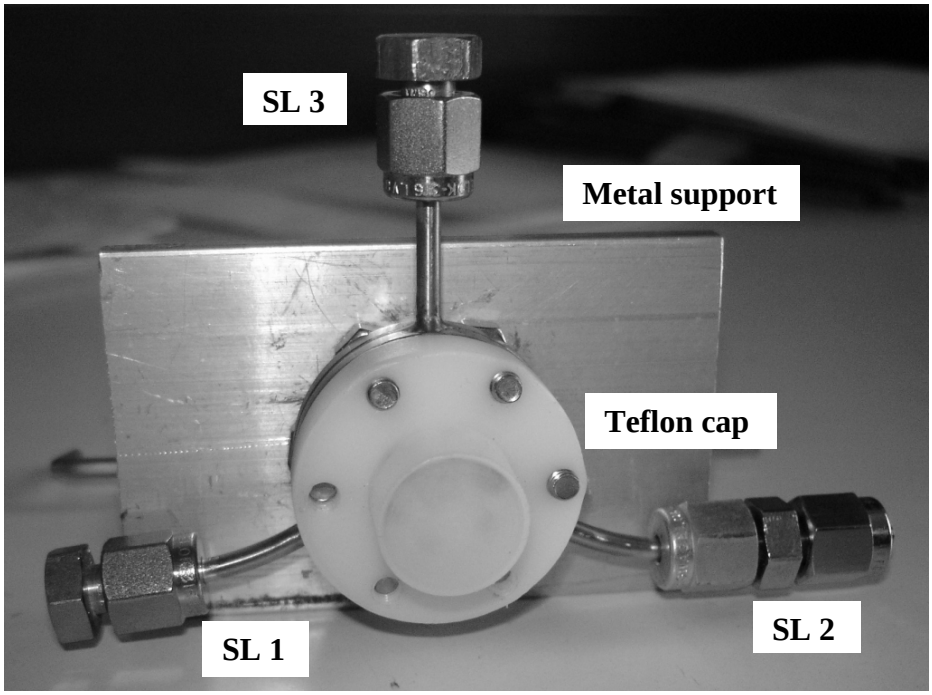

SL = Swage lock
Figure 2.26: Front view of the XAFS cell mounted on the stainless steel metal support

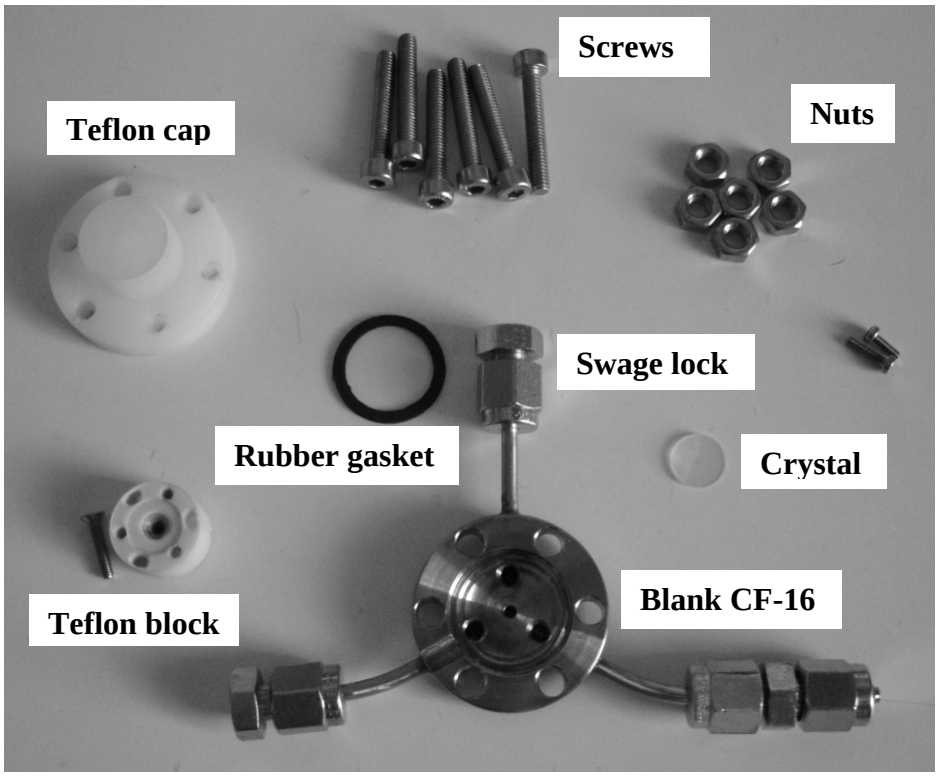

Figure 2.27: Item by item view of the XAFS cell showing the various components used for its construction.

In order to carry out XAFS measurements using the cell, an evacuated and well stoppered flask containing a solution of the complex was taken to a glove box together with the cell as shown in figure 2.27. The cell was then coupled up in the glove box. First the Teflon block and crystal were screwed in place, and then a few micro liters of the complex were dropped on the crystal surface and allowed to dry off. The cap was screwed in place and the apparatus was mounted on the beam line using a goniometer. The two ridges on the metal support were used for fine alignment in the beam.

In order to test whether the cell was air- and vacuum-tight, we exploited the sensitivity of the allyl complex to air. After recording a spectrum of Mo K-edge using the closed cell, we removed the teflon cap and rescanned the surface under the same conditions. As expected, the second spectrum was visibly different from the first one, an indication that the allyl groups had undergone significant chemical transformation in air. In fact, we used this test to verify the structural integrity of all Mo-allyl samples we investigated using XAFS and it was from one such test that we found out that a sample sent to us from a different

laboratory had actually decomposed. It was based upon this experience that we decided to synthesise the Mo-allyl complex ourselves.

2.12 The Elements

2.12.1 Aluminium

Aluminium falls in the third group of elements in the periodic table alongside boron (B), gallium (Ga), indium (In) and thallium (Th) and has the electronic configuration [Ne] $3s^2$, $3p^1$. Al is the most abundant metal and the third most abundant element (after oxygen and silicon) by weight on the earth's crust. The most important ore of aluminium is bauxite, which is a generic name for several minerals with formulae varying between $Al_2O_3.H_2O$ and $Al_2O_3.3H_2O$[59]. It also occurs in large amounts in rocks as feldspars and micas in the form of aluminosilicates and as cryolite (Na_3AlF_6)[60].

Aluminium is obtained from the ore bauxite which may be AlO.OH, $Al_2O_3.H_2O$, and $AlOH_3.3H_2O$. The largest sources are Australia (36 %), Guinea (17 %), Brazil (8 %), Jamaica (7%) and the former Soviet Union (6%)[59]. The first step in its extraction involves the purification of the ore to the oxide Al_2O_3, which is then extracted to the metal by the *Hall-Héroult* process. Naturally occurring aluminium is almost 100% composed of the $^{27}_{13}Al$ isotope[61].

Aluminium is relatively soft and weak in pure state, but is much stronger when alloyed with other metals. The alloys of aluminium include magnalium (10-30% Mg), duralumin (Mg, Al, Cu), aluman (Al, Mn), constructal (Al, Zn, Cu, Mg), skleron (Al, Zn), etc. find applications in[61]:

a. the aircraft, ship, and car industries
b. containers such as canned drinks, tubes for tooth paste, metal foil, etc
c. electric cables
d. fine Al powder is used in paints, explosives and fireworks
e. cooking utensils
f. construction industry.

The most important oxide of Al is alumina, Al_2O_3. It can be made by dehydrating $Al(OH)_3$, or from the elements. The two most known polymorphs are the α- and γ-Al_2O_3. The α-type, which is also known as corundum and exists as a mineral, can be made by heating γ-Al_2O_3 above 1000 °C. The crystal structure of corundum is hexagonally close-packed oxygen atoms, with two thirds of the octahedral holes filled by Al^{3+} ions[59,60]. γ-Al_2O_3 on the other hand can be prepared by dehydrating $Al(OH)_3$ below 450 °C and is sometimes referred to as the defect "spinel" structure. The oxide that forms on the surface of the metal has another structure, namely, a defect rock salt structure; there is an arrangement of Al and O ions in the rock salt mode with every third Al ion missing[60]. A form of Al_2O_3, called β-alumina, normally contains alkali metal ions and has the ideal position $M_2O.Al_2O_3$[62].

Toxicologically, aluminium is believed to be non-toxic to humans. $Al(OH)_3$ is widely used as an anti-acid treatment for indigestion. The sulphate, $Al_2(SO_4)_3$ is used for the treatment of drinking water. However, it is not completely harmless as studies have shown that it shows acute toxicity to people with kidney failures. Deposits of aluminium salts have also been discovered in the brains of Alzheimer patients[59].

2.12.2 Chromium

Chromium belongs to the short group of elements named after the element itself. The Chromium group comprises the elements Cr, Mo and W. Cr, with the electronic configuration [Ar] $3d^5$ $4s^1$ can accommodate oxidation states from -2 to +6, with the most abundant and stable ones being the +2, +3 and +6 states. The +2 state is reducing, whilst the +6 is strongly oxidising.

Chromium occurs in nature as chromite, $FeCr_2O_4$. This ore is the chromium analogue of magnetite Fe_3O_4. Chromite has a spinel structure with the O atoms arranged in a cubic close-packed lattice with Fe^{2+}in one eighth of the available tetrahedral holes and Cr^{3+} in one quarter of the tetrahedral holes. The largest sources of chromite are found in South Africa (36%), former USSR (28%), Turkey (7%), India, Albania, Finland and Zimbabwe (ca. 17%)[59]. The extraction of chromium involves several steps, the first one being the

conversion of chromite to dichromate, then reduction in coke to the oxide, followed by reduction with Al in the thermite reaction.

$$2FeCr_2O_4 + 8NaOH + 7/2O_2 \xrightarrow{1100\ °C} 4Na_2[CrO_4] + Fe_2O_3 + 4H_2O$$

$$Na_2[CrO_4] + H^+ \longrightarrow Na_2[Cr_2O_7]$$

$$Na_2[Cr_2O_7] + 2C \longrightarrow Cr_2O_3 + Na_2CO_3 + CO$$

$$Cr_2O_3 + Al \longrightarrow 2Cr + Al_2O_3$$

The above extraction method is applied only when pure chromium is required. Otherwise, the extraction method is carried out in a single step in a furnace using coke[60].

$$FeCr_2O_4 + 4C \longrightarrow Fe + 2Cr + 4CO$$

Chromic (Cr^{3+}) compounds are the most important and stable compounds of chromium. Cr_2O_3 is a green solid which is used as a pigment. Cr_2O_3 and Cr supported on other oxides such as Al_2O_3 catalyses a wide range of reactions[59]. It is prepared by burning the metal in air or by heating CrO_3. The oxide has the Al_2O_3 corundum structure. This shared structural property between the two oxides was one important factor that led to the use of a Cr single crystal for the epitaxial growth of Al_2O_3 (see section 3.1).

Industrially, chromium is used as a protective coating because of its extreme resistance to ordinary corrosive agents. Biologically, chromium is of significant importance in mammals. Cr^{3+} and insulin are both responsible for regulating blood sugar levels. Some cases of diabetes may reflect faulty Cr metabolism. The most important toxicological form of Cr is the Cr^{6+}. Large amounts of Cr salts containing this ion either ingested or in contact with the skin are carcinogenic[59]. This fact was exploited by the US film industry Hollywood in 2001 in the blockbuster movie “Erin Brokovich” starring Julia Roberts. In the movie, Roberts, a normal house wife, confronts the authorities of a near-by chemical plant that dumps waste containing Cr(VI) in the environment leading to pollution of the drinking water.

2.12.3 Molybdenum

Molybdenum, the second element in the chromium group, has the atomic number 42 and an electronic configuration of [Kr] $4d^5$ $5s^1$. Its chemistry is therefore dominated by the ability to loose all five d-electrons as well as the s-electron.

Molybdenum occurs in nature as molybdenite MoS_2. It can also occur as molybdate $PdMoO_4$ and $MgMoO_4$. It is extracted by roasting the sulphide to MoO_3. This may be added to steel directly, or may be heated with Al, Fe to give ferromolybdenum. Pure Mo is obtained by dissolving MoO_3 in dilute ammonium hydroxide[59,60].

Almost 90% of molybdenum is used to make cutting steel and stainless steel. It is also used as a catalyst in the petrochemical industry and organic derivatives of the element catalyse a whole range of reactions (see table 1). MoS_2 is a good lubricant, either on its own or when mixed with hydrocarbon oil. Biologically, Mo is one of the most active transition elements[59,63] and the most recognised role is the one it plays in the catalysts of nitrogen fixing (conversion of atmospheric N_2 to NH_3) bacteria. These bacteria are believed to contain proteins called molybdoferredoxin.